8. Lasers

Laser is an acronym for ***L***ight ***A***mplification by ***S***timulated ***E***mission of ***R***adiation that describes the basic physical principle of its operation. *Gordon*, *Zeiger* and *Townes* [8.1] showed for the first time in 1955 that a microwave could be amplified by NH_3 molecules on the inversion transition at $\lambda = 1.26\,\text{cm}$ (Fig. 4.13) if these molecules were prepared in such a way that the upper level of the transition had a larger population than the lower one. With such inverted NH_3 molecules inside a microwave cavity, the first "maser" (microwave amplification by stimulated emission of radiation) could be operated.

Schawlow and *Townes* published a paper in 1958 with detailed discussions of how the maser principle might be extended into the visible spectral range [8.2]. The first experimental realization of a laser was demonstrated in 1960 by *Maiman*, who built a ruby laser, which was pumped by a helical flashlamp and emitted coherent radiation at $\lambda = 694\,\text{nm}$ [8.3].

Since then, lasers have been developed spanning the whole spectral range from the far infrared down to the vacuum ultraviolet region. They have proved to be valuable tools not only for the solution of many scientific problems but also for numerous technical applications.

In this chapter we will discuss the basic physical principles of lasers, the most important classes of lasers and some interesting novel applications. More detailed discussions can be found in the vast literature on lasers [8.4, 5, 6].

8.1 Physical Principles

A laser basically consists of three components (Fig. 8.1):

1. The ***active medium*** where an inverted population $N(E)$ is created by selective energy transfer.

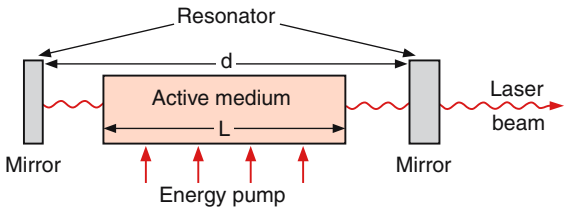

Fig. 8.1. Schematic setup of a laser

   This population distribution $N(E)$ deviates strongly from a thermal Boltzmann distribution (Fig. 8.2) in such a way that $N(E_i) > N(E_k)$ for $E_i > E_k$, contrary to a thermal population

$$N(E) \propto \mathrm{e}^{-E/kT} .$$

2. The ***energy pump***, (flashlamp, gas discharge, electric current or another laser) that generates the population inversion.
3. The ***optical resonator*** that stores the fluorescence emitted by the active medium in a few modes of the radiation field (see below). In these modes the photon number becomes $N_{\text{phot}} \gg 1$. Therefore, in these modes, the induced emission becomes much larger than the spontaneous emission (see Sect. 7.1.1).

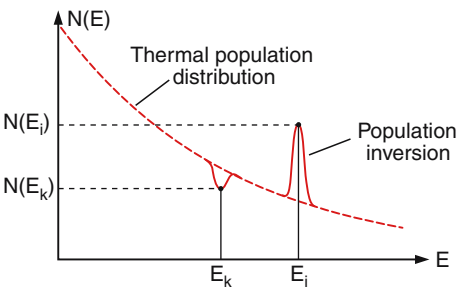

Fig. 8.2. Selective population inversion ($N_i > N_k$) in spite of $E_i > E_k$, deviating from a thermal population distribution (*red dashed* curve)

The optical resonator furthermore reflects the induced emission back into the active medium and allows many paths back and forth through the medium, thus realizing a long amplification path. This converts the light amplifier into a light oscillator if the total amplification exceeds the total losses.

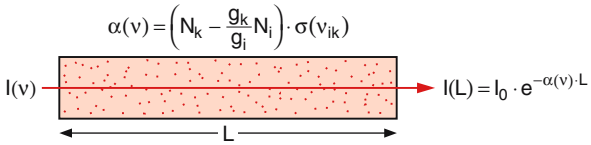

Fig. 8.3. Attenuation ($\alpha > 0$) or amplification ($\alpha < 0$) of a light wave passing through a medium

8.1.1 Threshold Condition

When an electromagnetic wave with frequency ν travels in the z direction through a medium (Fig. 8.3) its intensity changes according to Beer's absorption law

$$I(\nu, z) = I(\nu, 0) \cdot \mathrm{e}^{-\alpha(\nu)\cdot z} \,. \tag{8.1}$$

The frequency-dependent absorption coefficient

$$\alpha(\nu) = [N_k - (g_k/g_i)N_i]\sigma(\nu) \tag{8.2}$$

is determined by the absorption cross section $\sigma(\nu)$ of the transition $N_k \rightarrow N_i$, the population densities N_i, N_k, of the levels with energies E_i, E_k with $\Delta E = E_i - E_k = h\nu$, and their statistical weights g_i, g_k (the statistical weight of a level with total angular momentum quantum number J is $g = 2J + 1$). For

$$N_i > (g_i/g_k)N_k \Rightarrow \alpha(\nu) < 0 \tag{8.2a}$$

this means that the transmitted wave will be amplified instead of attenuated. Such a deviation (8.2a) from a thermal equilibrium population is called ***inversion*** and the medium where this inversion is realized is called the ***active medium***.

When the active medium with length L is placed between two parallel mirrors (Fig. 8.1) the light wave is reflected back and forth and passes through the active medium many times, where it is amplified each time by the factor

$$G(\nu) = \frac{I(\nu, 2L)}{I(\nu, 0)} = \mathrm{e}^{-2\alpha(\nu)\cdot L} \,, \tag{8.3}$$

which is larger than 1 for $\alpha(\nu) < 0$.

Unfortunately there are also losses that attenuate the wave. These are reflection, diffraction, absorption, and scattering losses.

Reflection losses. A mirror with reflection coefficient R only reflects the fraction $R < 1$ of the incident intensity. If absorption losses of the mirror can be neglected, the fraction $(1 - R)$ of the incident intensity is transmitted through the mirror.

Absorption and scattering losses. In case of gas lasers, the windows of the tube containing the active medium may absorb and scatter some of the transmitted light. For solid lasers the end surfaces of the laser rod may scatter and reflect some light. Also, the active medium might not have a spatially uniform inversion, leaving locations with $\alpha > 0$. Finally, the mirror surfaces are not perfect. They can scatter light and the reflecting layers can also show small absorptions.

Diffraction losses. Depending on the parameters of the optical resonator (aperture diameter a, mirror separation d and radius of curvature r of the mirrors) the wave being reflected back and forth shows an angular spread due to diffraction (see below). This means that only part of the intensity is reflected back into the active medium, which represents a diffraction loss per roundtrip through the resonator.

We will describe the sum of all these losses per roundtrip by the loss factor γ. The intensity after one roundtrip has decreased (without amplification by the active medium) by the factor $\mathrm{e}^{-\gamma}$:

$$\frac{I(2d)}{I(0)} = \mathrm{e}^{-\gamma} \quad \text{with} \quad \gamma = \gamma_\mathrm{r} + \gamma_\mathrm{sc} + \gamma_\mathrm{dif} \,. \tag{8.4}$$

Taking into account the amplification by the active medium we obtain the gain factor

$$G(\nu) = \frac{I(\nu, 2d)}{I(\nu, 0)} = \mathrm{e}^{-(2\alpha(\nu)\cdot L + \gamma)} \,. \tag{8.5}$$

For $G(\nu) > 1$ the amplification overcomes the losses and the light amplifier becomes a light oscillator. According to (8.2) and (8.5) the threshold condition for starting the self-sustained oscillation (i. e., the laser oscillator) is

$$2\alpha(\nu) \cdot L + \gamma \leq 0 \,. \tag{8.5a}$$

Inserting (8.2) this gives

$$2[N_k - (g_k/g_i)N_i] \cdot \sigma(\nu) \cdot L + \gamma \leq 0 \,. \tag{8.5b}$$

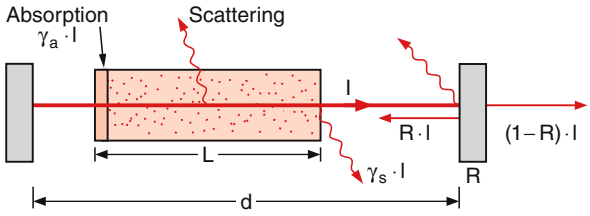

Fig. 8.4. Illustration of the losses in a laser resonator

The minimum inversion $\Delta N = N_i(g_k/g_i) - N_k$ for lasing must therefore fulfill the threshold condition

$$\Delta N = N_i(g_k/g_i) - N_k \geq \Delta N_{\text{thr}} = \frac{\gamma(\nu)}{2\sigma(\nu) \cdot L} \quad . \tag{8.6}$$

If the energy transfer from the pump into the active medium is sufficiently strong to achieve $\Delta N > \Delta N_{\text{threshold}}$ the light will be amplified for each roundtrip, because the amplification exceeds all losses.

The laser oscillation for a continuous laser with time-independent pump power builds up in the following way.

Fluorescence photons, spontaneously emitted by the upper level E_i into the direction of the resonator axis are reflected back into the active medium, where they are amplified, reflected back into the medium by the rear mirror, etc. This results in a photon avalanche with increasing photon number after each roundtrip, if $G(\nu) > 1$ (Fig. 8.5). Part of this radiation power, circulating between the two resonator mirrors is transmitted by one of the mirrors. With increasing photon number the probability of induced emission increases, which decreases the population inversion until it is depleted down to the threshold value. Here, gain and losses are just equal and the laser has reached its stationary state, where the emission is constant. The emitted laser power depends on the pump power and the pumping efficiency.

For pulsed lasers the pump power is time-dependent. After a certain pumping time the threshold inversion has been reached. Now laser oscillation starts, which depletes the inversion due to induced emission. The time dependence of the laser output power depends on the relative rates $+\mathrm{d}N_i/\mathrm{d}t$ of pumping and $-\mathrm{d}(N_i - N_k)/\mathrm{d}t$ of inversion depletion by induced emission. For sufficiently strong pumping the laser output power follows the time-dependent pump power and a laser pulse is emitted that is shorter than the pump pulse because it only starts after inversion has been reached and ends when the pump power falls below the threshold value (Fig. 8.6).

In cases of strong depletion by stimulated emission the inversion drops below the threshold already during the pump pulse and the laser emission stops, until the pump has again built up sufficient inversion. Now the laser emission starts again. In such cases (e. g., for the ruby laser) the laser output consists of more or less irregular spikes with short durations, which are emitted while the pump power is above threshold (Fig. 8.7).

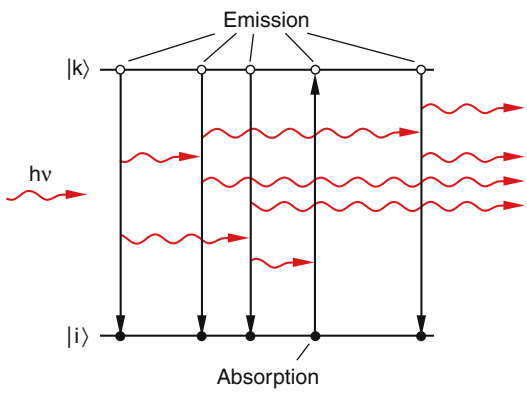

Fig. 8.5. Photon avalanche generated by a photon passing through the active medium due to induced emission

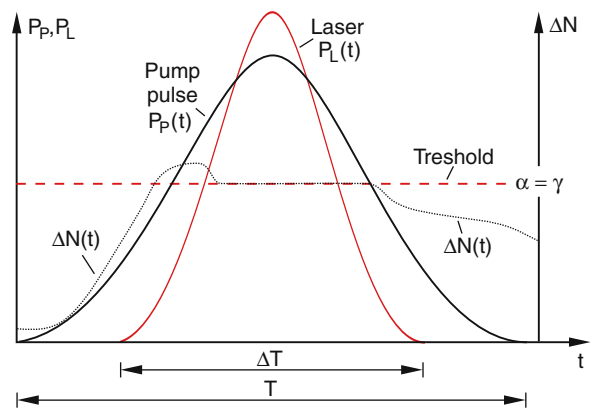

Fig. 8.6. Pump-pulse power $P_P(t)$, laser power $P_L(t)$, threshold inversion $\alpha = \gamma$ and time-dependent inversion $\Delta N(t)$ for a pulsed laser

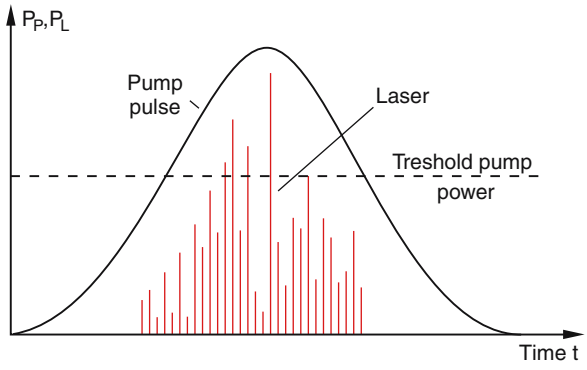

Fig. 8.7. Schematic illustration of spikes in the output of a flashlamp-pumped solid-state laser with long relaxation times τ_i, τ_k

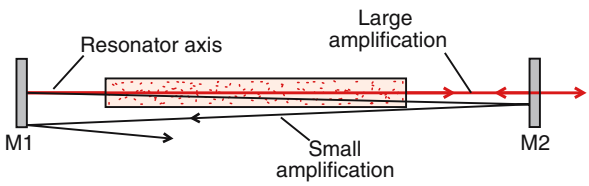

Fig. 8.8. The net gain depends on the effective path length through the active medium

The amplification factor is largest for photons with the longest path through the active medium. These are those photons that travel along the resonator axis. Photons emitted into directions inclined to the axis, are not reflected back into the active medium and are therefore less amplified (Fig. 8.8). If their amplification does not reach the threshold value, they cannot contribute to the laser oscillation. Depending on the geometric dimensions of the active medium and the limiting apertures of the optical resonator the laser oscillation is restricted to a small angular divergence around the resonator axis. This results in a laser beam, transmitted through one of the resonator mirrors, which has a small divergence and appears in many cases as nearly parallel light beam with a small diameter.

8.1.2 Generation of Population Inversion

The minimum inversion, required for laser oscillation, can be achieved by a selective pump process, that populates the upper level E_i of the laser transition more strongly than the lower level E_k. The pump energy can be transferred either as a pulse (e. g., by flashlamps) or continuously (e. g., by electron impact in a stationary gas discharge). In the first case, laser emission occurs as a pulse, in the second case it occurs continuously (cw = continuous wave operation). We will provide examples of both cases.

The flashlamp-pumped ruby laser historically represents the first demonstration of pulsed laser operation. Its active medium is a cylindrical rod consisting of an Al_2O_3 crystal, that is doped with about 1% Cr^{+++} ions. The level scheme of these Cr^{+++} ions is shown in Fig. 8.9. By absorption of light from the flashlamp the ions are pumped from the ground state E_0 into the levels E_1 and E_2, which are strongly broadened by interaction with the host crystal. The resulting broad absorption lines overlap with the maximum of the spectral continuum emitted by the flashlamp filled with xenon and can therefore be effectively pumped. The two upper levels transfer part of their excitation energy in a very short time (10^{-10}–10^{-11} s) to vibrational energy of the crystal due to a strong interaction with their surroundings. This loss of excitation energy results in fast radiationless transitions into a sharp lower level E_i, which is the upper level of the laser transition $E_i \rightarrow E_0$ at $\lambda = 694$ nm.

In order to achieve population inversion, the number of Cr^{+++} ions in the level E_i must be larger than that in the ground state E_0. A direct pumping of level E_i on a transition $E_0 \rightarrow E_i$ could not achieve inversion, because as soon as the populations of both levels become equal, the absorption of the pump light on the laser transition becomes zero and the pump can no longer populate level E_i. The intermediate levels E_1 and E_2 are therefore essential for the realization of laser oscillation. One needs at least three levels, as indicated in

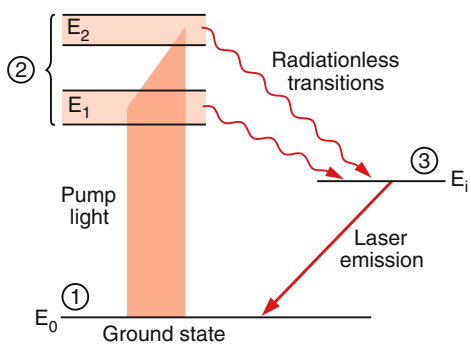

Fig. 8.9. Level scheme of the ruby laser

Fig. 8.9 by the encircled numbers (where E_1 and E_2 have been combined into a single level). Such a level scheme for laser operation is called a three level system. The ruby laser is therefore a ***three level laser***.

Note:

Under special conditions it is also possible to achieve inversion for a short time in a two-level system, if the pumping time is short compared to all relaxation times of the system and even shorter than the Rabi oscillation time $T_R = \pi \cdot h/(\boldsymbol{M}_{ik} \cdot \boldsymbol{E}(\nu_{ik}))$, where $\boldsymbol{M}_{ik}$ is the matrix element for the transition $i \rightarrow k$ and $\boldsymbol{E}$ is the electric field vector of the pump wave. These conditions, however, apply only to very few real systems that are specially designed.

There are several possible experimental configurations of the ruby laser using linear or helical flashlamps (Fig. 8.10). While *Maiman* used the helical design for his first laser, nowadays the linear configuration is preferred. Here the cylindrical ruby rod and the linear flashlamp are placed along the two focal lines of a cylindrical reflector with elliptical cross section (Fig. 8.10a). The light emitted by the flashlamp is focused into the ruby rod from all sides, due to the imaging characteristics of the pump light reflector with elliptical cross section. The mirror surface is coated with dielectric layers with maximum reflection at those wavelengths preferentially absorbed by the Cr^{+++} ions on the transitions $E_0 \rightarrow E_1$, E_2. The parallel end faces of the ruby rod are polished and one end face is coated with a highly reflecting layer, the other endface for the laser output with a partially transmitting layer. The flashlamp is fired by discharging a high voltage capacitor through the lamp. While the pump pulse lasts for approximately 1−3 ms, the laser output is a pulse of typically 0.2−0.4 ms, generally consisting of many short ($\approx 1\,\mu$s) spikes.

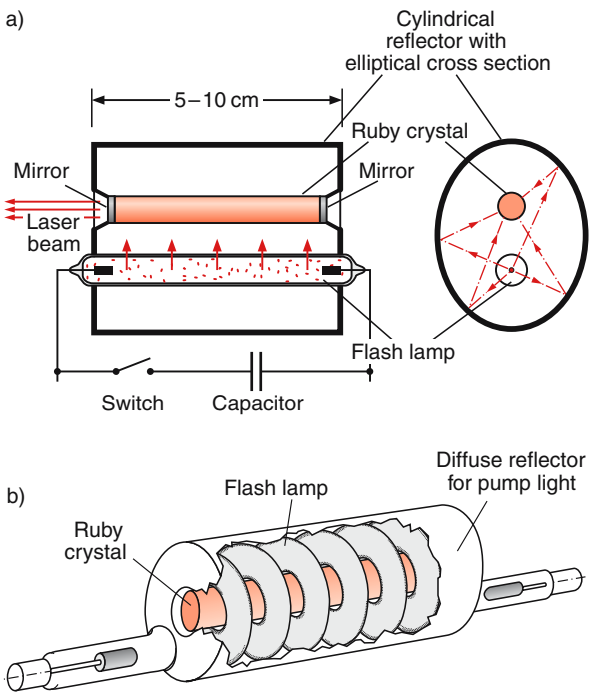

Fig. 8.10a,b. Two possible configurations for a pulsed ruby laser. (**a**) Linear flashlamp with cylindrical reflector cavity with elliptical cross section (**b**) Helical flashlamp, originally used by *Maiman* for his first ruby laser

Our second example is the He-Ne-laser, which represents the most commonly used cw gas laser. This laser is based on a four-level system and the pumping is achieved by inelastic collisions of electrons with helium and neon atoms in a stationary gas discharge in a glass tube. Its principle design is shown in Fig. 8.11. A gas discharge is initiated by a high voltage between a cylindrical anode and an aluminum cathode surrounding a glass or quartz capillary (1−4 mm diameter). The power supply for a He-Ne laser has a typical output of 5−10 mA at a voltage of 1 kV. The whole tube is filled with a mixture of about 88% He and 12% Ne at a total pressure of 1−5 mbar. In this discharge (in particular in the narrow capillary, where the current density is high), He and Ne atoms are excited into many high lying energy levels. Most of these levels have a short lifetime and decay by spontaneous emission. In the helium atom there are two metastable

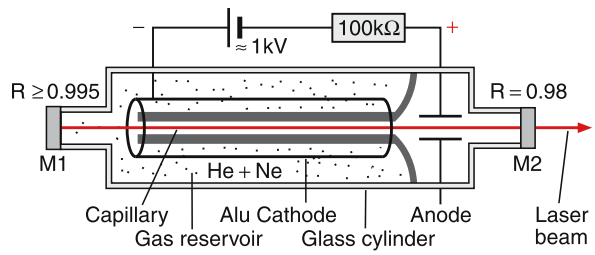

Fig. 8.11. Design of a He-Ne laser

states with long lifetimes (see Sect. 6.2). These are the $2\,^3S_1 (\tau = 20\,\text{ms})$ state and the $2\,^1S_0$ state ($\tau \geqslant 600\,\text{s}$), which cannot decay by allowed dipole transitions into lower states. They are populated not only by electron impact but also by cascading spontaneous emissions from higher levels (Fig. 8.12). In the discharge, therefore, a high concentration of He-atoms in these states is built up. The electron configuration of excited states in neon is $1s^2\,2s^2\,2p^5\,n'l'$, with $n' = 3, 4, 5, \ldots$. In "Paschen-notation" (L-S-coupling) the sublevels of each configuration are numbered with decreasing energy. For example the $2p^5\,3p$ configuration has ten sublevels $^{2S+1}L_J$, which are (with decreasing energy) $^1S_0, ^3P_1, ^3P_0, ^3P_2, ^1P_1, ^1D_2, ^3D_1, ^3D_2, ^3D_3$ and $^3S_1$ numbered by $1, 2, \ldots 10$.

Both metastable He states are in close energy resonance with excited neon levels. By collisions between excited He atoms and ground state Ne atoms this energy resonance results in large cross sections for the collisional transfer of the excitation energy from the He to the Ne atoms (near resonance collisions of the second kind) according to the scheme:

$$\begin{aligned} \text{He}^*(2\,^1S_0) + \text{Ne}(2\,^1S_0) &\rightarrow \text{He}(1\,^1S_0) + \text{Ne}^*(5s) \\ \text{He}^*(2\,^3S_1) + \text{Ne}(1^1\,S_0) &\rightarrow \text{He}(1\,^1S_0) + \text{Ne}^*(4s) \end{aligned} \tag{8.7}$$

This energy transfer results in a selective excitation of the neon levels $4s$ and $5s$, which achieve a higher population than the lower levels $4p$ and $5p$, resulting in a population inversion on the transitions $5s \rightarrow 5p$ ($\lambda = 3.39\,\mu\text{m}$), $4s \rightarrow 4p$ ($\lambda = 1.15\,\mu\text{m}$) and $5s \rightarrow 4p$ ($\lambda = 633\,\text{nm}$). Such a system, where the laser transition occurs between two excited states, and four levels are involved (the He ground state, a metastable He state and the two Ne levels) is called a ***four-level system***.

Since the population of the lower laser levels is very small, only a small percentage ($\approx 10^{-5}$) of all He atoms needs to be excited into the metastable states, contrary to the three level system of the ruby laser where more than 50% of all Cr^{+++}-ions had to be pumped into the upper laser level. Therefore only about 10^{-6} of all neon atoms occupy the upper levels of the laser transitions.

The level scheme shows that laser oscillation is possible for several transitions with different wavelengths. However, only those transitions can reach laser threshold, for which the gain exceeds the losses. The losses can be selected by a proper choice of the resonator mirrors. If the reflection of these mirrors is high for one wavelength but low for the others, laser oscillation can only occur at this favored wavelength.

The gain on the transition $5s \rightarrow 4p$ ($\lambda = 633\,\text{nm}$) reaches only a few percent for a length of 20 cm in the active medium. Therefore the losses have to be correspondingly low and laser operation could only be achieved after high reflecting dielectric mirrors had been designed with reflectivities of 99.99% for one mirror and 98% for the transmitting mirror. The gain can be increased by using the isotope ^{3}He instead of ^{4}He, because here the energy resonance between the metastable He levels and the excited Ne levels is even closer than in ^{4}He and therefore the cross section for energy transfer from He to Ne is larger.

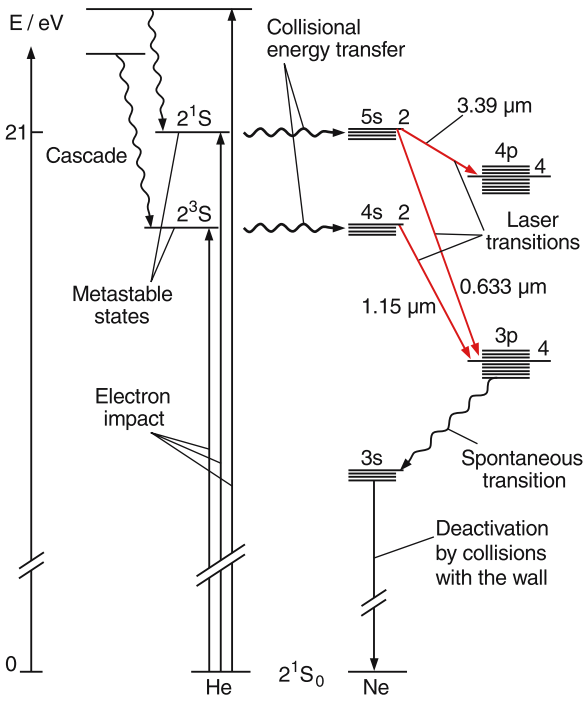

Fig. 8.12. Level scheme of the He-Ne laser with three possible laser transitions

8.1.3 The Frequency Spectrum of Induced Emission

Both the gain $-\alpha(\nu) \cdot L$ and the losses $\gamma(\nu)$ depend on the frequency ν of the light wave. When the pump process starts, the laser reaches the threshold first for those

frequencies where the threshold inversion ΔN_{thr} is minimum. The frequency dependence of the gain depends on the active medium. For gaseous media (He-Ne-laser, Ar^+-laser) the spectral lines are Doppler-broadened, showing a Gaussian line profile with a width of several GHz (10^9 Hz). For solid state lasers or liquid lasers the line width is mainly determined by interaction of the laser atoms, ions or molecules with their surroundings. It is generally much broader than in gases.

The loss factor γ mainly depends on the characteristics of the optical resonator. It has minima at the resonance frequencies of the resonator. Therefore lasing starts at those resonator resonances that lie within the spectral gain profile of the active medium. If the spacing between resonator modes is smaller than the spectral width of the gain profile, the laser oscillates on several wavelengths simultaneously. This deteriorates the coherence properties of the laser emission. If oscillation on a single wavelength is required, additional wavelength selecting elements have to be introduced. This can be realized either by a special resonator design or by prisms or optical gratings inside or outside the resonator.

Since the laser resonator plays a central role for the spectral characteristics of laser emission, we will first discuss optical resonators.

8.2 Optical Resonators

In Sect. 3.1.2 it was shown that inside a closed resonator a radiation field can exist with an energy density $w_\nu(\nu)$ that is equally distributed over all resonances or modes of the cavity. In the optical spectral range where the wavelength λ is small compared to the dimensions of the cavity, the number of modes within the frequency interval $\mathrm{d}\nu$ is (see (3.10b))

$$n(\nu)\,\mathrm{d}\nu = 8\pi(\nu^2/c^3)\,\mathrm{d}\nu\,.$$

For $\nu = 5\times10^{14}\,\mathrm{s}^{-1}$ ($\lambda = 600\,\mathrm{nm}$) the number of modes within a Doppler broadened spectral line ($\Delta\nu = 10^9\,\mathrm{s}^{-1}$) is $n(\nu)\Delta\nu = 2.5\times10^{14}\,\mathrm{m}^{-3}$. This implies that the spontaneous emission from excited atoms inside a closed cavity is distributed over many modes, which means that the average photon number per mode is very small. In such a closed cavity the induced emission, started by spontaneous photon avalanches, is spread out over many modes. Because the total power emitted by spontaneous and induced emission has to be supplied by the pump energy, one needs an exceedingly high pump power in order to achieve laser oscillation on all these modes. The laser emission would then be distributed over many directions into the solid angle 4π and the directionality of laser emission would be lost.

> Closed cavities, which are used for the realization of masers in the microwave region, where λ is comparable with the cavity dimensions, are not suitable for optical lasers.

8.2.1 The Quality Factor of Resonators

Assume that the kth resonator mode contains the radiation energy $W_k(t)$. If no energy is fed from external sources into this mode, its stored energy will decrease as

$$\frac{\mathrm{d}W_k}{\mathrm{d}t} = -\beta_k \cdot W_k\,, \tag{8.8}$$

which yields the time-dependent stored energy

$$W_k(t) = W_k(0)\cdot \mathrm{e}^{-\beta_k t} \tag{8.9}$$

with the loss factor β_k. After the time $\tau = 1/\beta_k$ the energy stored in the kth mode has decayed to $1/e$ of its initial value at $t = 0$. This time can be regarded as the mean lifetime of a photon stored in this resonator mode. We define the quality factor Q_k of the kth resonator mode as 2π times the ratio of the energy, stored in this mode to the energy loss per oscillation period $T = 1/\nu$ of the radiation with frequency ν:

$$Q_k = -\frac{2\pi\nu\cdot W_k}{\mathrm{d}W_k/\mathrm{d}t}\,. \tag{8.10}$$

Inserting (8.8) and (8.9) gives the relation between the loss factor β_k and the quality factor Q_k:

$$Q_k = -2\pi\nu/\beta_k\,. \tag{8.11}$$

The loss factor γ per roundtrip is then

$$\gamma_k = \beta_k\cdot(2d/c)\,. \tag{8.12}$$

Even if at $t = 0$ the radiation energy, supplied by spontaneous emission, is the same for all modes, those modes with a high Q-factor will store this energy for a longer time while those with a low Q-factor loose their energy after a short time.

8.2.2 Open Optical Resonators

In order to concentrate the induced emission onto a few modes, the Q-factor of the resonator must be large for these modes (i. e., the losses must be small), while it should be sufficiently small for all other modes, so that for a given pump power the threshold for laser oscillation is not reached for these modes.

Open resonators, consisting of a suitable arrangement of optical mirrors can fulfill this condition. We will illustrate this by the example of two plane-parallel mirrors M_1 and M_2 with reflectivity R_1 and R_2 and with diameters $2a$, which are separated by the distance d (Fig. 8.4). This represents, in fact, a Fabry-Perot interferometer (FPI) used in spectroscopy as a spectral filter with high resolution. There is, however, an essential difference from conventional FPI, where the mirror separation d is small compared to the diameter $2a$ of the mirrors. For this laser resonator the situation is the opposite: here $d \gg 2a$. This makes a large difference with respect to diffraction, which is negligible in a conventional FPI, but essential in a laser resonator.

We will first regard the reflection losses.

A light wave reflected back and forth between the mirrors suffers reflection losses and its intensity decreases per roundtrip according to

$$I(2d) = I_0 R_1 R_2 = I_0 \cdot \mathrm{e}^{-\gamma_\mathrm{r}} \,. \tag{8.13}$$

The reflection loss factor γ_r is defined as

$$\gamma_\mathrm{r} = -\ln(R_1 R_2) \,. \tag{8.14}$$

Since the transit time for one roundtrip is $T = 2d/c$, the mean lifetime τ of a photon stored in the resonator and traveling along the resonator axis is

$$\tau = \frac{2d}{c \cdot \ln(R_1 R_2)} \tag{8.15}$$

if no other losses were present.

EXAMPLE

$R_1 = 1$, $R_2 = 0.98$, $d = 0.5\,\mathrm{m} \Rightarrow \gamma_\mathrm{r} = 0.02$ and $\tau = 1.5 \times 10^{-7}\,\mathrm{s}$.

We will now discuss the diffraction losses of open resonators.

Because of the finite diameter $2a \ll d$ of the mirrors diffraction losses are generally not negligible. This is illustrated by Fig. 8.13c. A plane wave traveling from below onto the mirror M_1 is no longer reflected as a plane wave but becomes divergent because of diffraction. This is completely analogous to a plane wave passing through an aperture with diameter $2a$ (Fig. 8.13b). Here the transmitted wave shows an intensity profile

$$I(\Theta) = I_0 \left(\frac{2J_1(x)}{x} \right)^2 \quad \text{with} \quad x = \frac{2\pi a}{\lambda} \sin\Theta \tag{8.16}$$

with a central maximum and higher diffraction orders (see textbooks on optics). The central diffraction maximum has an angular width between the first two nodes of the Bessel function $J_1(x)$ on both sides of the maximum at $x = 0$, which gives

$$\sin\Theta = 1.2\lambda/(2a) \Rightarrow \Theta \approx \lambda/(1.7a) \,. \tag{8.17a}$$

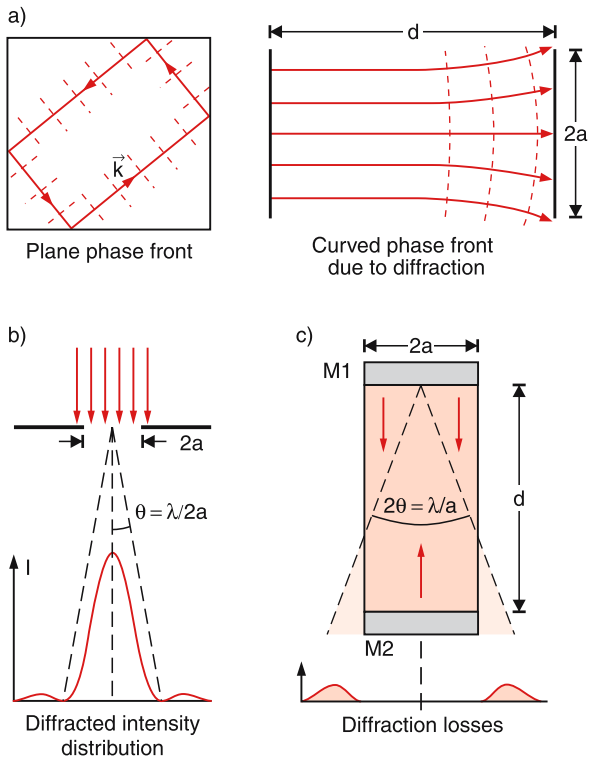

Fig. 8.13. (**a**) Plane waves as stationary field solutions in a cubic closed resonator compared with curved wave fronts in an open resonator with diffraction losses. (**b**) Diffraction pattern of a plane wave behind a circular aperture with diameter $2a$, compared in (**c**) to a similar pattern after reflection by a plane mirror of size $2a$

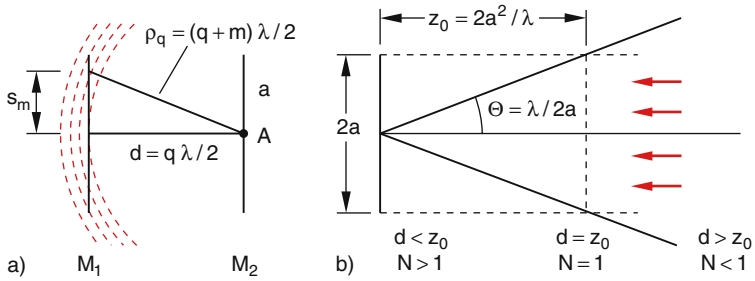

Fig. 8.14. (**a**) Fresnel zones on mirror M_1, as seen from the center A of the other mirror M_2. (**b**) The three regions of d/a with the Fresnel number $N > 1$, $N = 1$, and $N < 1$

Light with larger diffraction angles does not hit the mirror M_2 in Fig. 8.13c and is therefore lost. If the total light power included in the 0th diffraction order, should be reflected by M_2 the diffraction angle Θ has to obey the relation

$$\tan\Theta \cdot d \approx \Theta \cdot d \leq a\,.$$

Inserting (8.17a) yields

$$1.7\frac{a^2}{\lambda \cdot d} \geq 1\,. \tag{8.17b}$$

The ratio

$$N_F = a^2/(\lambda d) \tag{8.18}$$

is called the Fresnel number of the resonator. It gives the number of Fresnel zones on the surface of M_1, which can be seen from the center A of M_2 (Fig. 8.14).

A more detailed calculation shows [8.7, 8] that for $N_F \gg 1$ the diffraction loss factor is $\gamma_d \approx 1/N$. This means that in a resonator with Fresnel number N_F the light power drops after one roundtrip by a factor $\exp(-1/N)$ if only diffraction losses were present. When the light wave makes m roundtrips, the Fresnel number should be $N_F > m \cdot \gamma_R$ if the diffraction losses are to be smaller than the reflection losses.

EXAMPLE

For a FPI with $a = 2\,\text{cm}$ and $d = 1\,\text{cm}$, typically for spectroscopic applications, the Fresnel number for $\lambda = 500\,\text{nm}$ is $N_F = 8 \times 10^4$. The diffraction loss factor is $\gamma_d = 1.2 \times 10^{-5}$ and diffraction losses are therefore negligible. The phase fronts of a wave inside the FPI are planes and the mirror surfaces are nodes of the standing wave. These dimensions are, however, not suitable for a laser resonator.

The resonator of a gas laser with plane mirrors (diameter $2a = 0.2\,\text{cm}$ and a separation of $d = 50\,\text{cm}$) has for $\lambda = 500\,\text{nm}$ a Fresnel number $N_F = 4$. The diffraction losses per roundtrip amount already to 25% and a He-Ne-laser with such a resonator would not reach threshold.

8.2.3 Modes of Open Resonators

While the modes of closed cavities can be described as a superposition of plane waves (see Sect. 3.1.2) with amplitudes and phases that are constant on planes perpendicular to the wave vector $\boldsymbol{k}$, in open resonators both quantities are changing across these planes because the diffraction causes a curvature of the wave fronts. Possible modes of open resonators are therefore not plane waves!

The amplitude and phase distribution $A(x, y)$ and $\varphi(x, y)$ of modes in an open resonator with the resonator axis in z-direction can be determined in the following way.

The light wave being reflected back and forth between the two resonator mirrors corresponds to, regarding the diffraction effects, a wave passing through a series of equidistant apertures with the same size as the mirrors (Fig. 8.15). This is shown in optics by Babinet's theorem. When a plane wave passes through the first aperture in the plane $z = 0$ the amplitude distribution $A(x, y)$ will change due to diffraction. The amplitude will at first decrease more at the edges than in the center, until the diffraction losses are equal for all values of x and y. We assume that after having passed the nth aperture, the diffracted wave will have reached a stationary state, where the relative amplitude distribution $A(x, y)$ will no longer change, although the absolute total amplitude may still decrease. This implies the relation:

$$A_n(x, y) = C \cdot A_{n-1}(x, y) \tag{8.19}$$

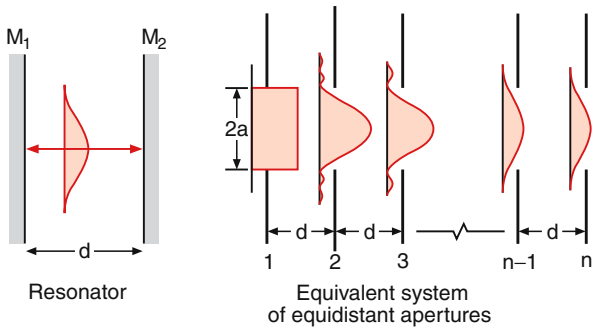

Fig. 8.15. The diffraction of a wave traveling back and forth between two mirrors M_1 and M_2 is equivalent to that of a wave passing through a series of equidistant apertures

where the constant C with $|C| < 1$ does not depend on x and y.

The amplitude distribution $A_n(x, y)$ across the nth aperture can be calculated from the distribution $A_{n-1}(x', y')$ across the foregoing aperture, using Kirchhoff's diffraction theory. The light emitted by every point (x', y') contributes to the amplitude $A(x, y)$ in the nth aperture. From Fig. 8.16 we obtain the relation

$$A_n(x, y) = -\frac{i}{2\lambda} \int_{x'} \int_{y'} A_{n-1}(x', y') \frac{1}{\varrho} e^{-ik\varrho} \times (1 + \cos\vartheta)\, dx'\, dy' . \qquad (8.20)$$

Inserting (8.19) gives an integral equation for the amplitude $A(x, y)$, which can be generally solved only numerical, except for special cases where analytical solutions are possible. The constant factor C in (8.19) is found to be

$$C = (1 - \gamma_d)^{1/2} \cdot e^{i\varphi} \qquad (8.21)$$

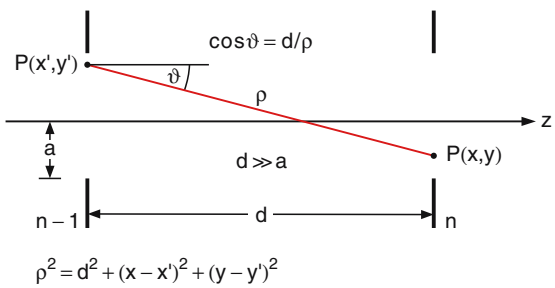

Fig. 8.16. Illustration of Eq. (8.20)

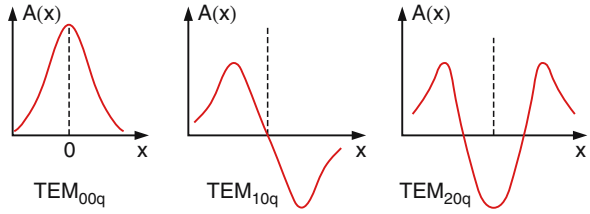

Fig. 8.17. One-dimensional electric field distribution in the x direction for some resonator modes

where γ_B is the diffraction factor, and φ is the phase shift, caused by the curvature of the wave fronts, due to diffraction.

Some solutions of the integral equation (8.20) are illustrated in Fig. 8.17. They correspond to stationary solutions as standing waves between the two resonator mirrors and are called transverse electromagnetic (***TEM***) modes of the open resonator. They are labeled by three indices, which give the number of nodes of the standing wave in the x-, y-, and z-directions (Fig. 8.18). The $TEM_{0,0,q}$ modes with no nodes in x- and y-direction are called ***fundamental modes***. Their

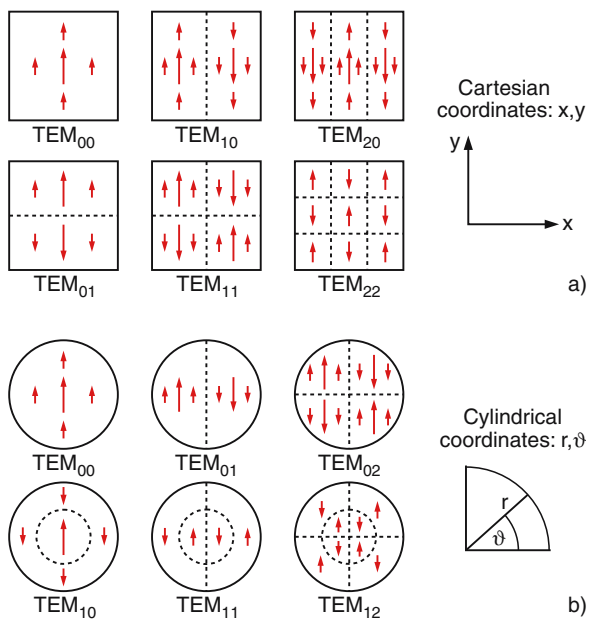

Fig. 8.18a,b. Schematic representation of electric field distribution in the xy-plane inside the resonator (**a**) In Cartesian coordinates (**b**) In cylindric coordinates

$\boldsymbol{k}$-vector points into the $\pm z$-direction and they have q nodes along the z-axis. Their electric field amplitude distribution $E(x, y)$ shows a Gaussian profile.

Generally, mirrors of circular size are used and the active medium also has a circular cross section. Because of this cylindrical symmetry, cylinder coordinates (r, φ, z) are better suited for the description of the amplitude distribution of the modes. The fundamental modes are then described by the radial field amplitude distribution

$$E(r, \varphi, z) = E_0 \, \mathrm{e}^{-(r/w)^2} \, ,$$

where w is the beam waist, i.e. for $r = w$ the amplitude has decreased to E_0/e. Because the intensity is related to the electric field amplitude by

$$I = c\varepsilon_0 E^2$$

we obtain the intensity distribution of the fundamental modes

$$I(r, z) = I_0 \, \mathrm{e}^{-2(r/w(z))^2} \qquad (8.22)$$

where the beam waist $r = w(z)$, for which the intensity has dropped to $I(w) = I(0)/\mathrm{e}^2$ can depend on the z-coordinate (Fig. 8.19).

The higher transverse modes $\mathrm{TEM}_{n,m,q}$ with $n, m > 0$ correspond to standing waves with $\boldsymbol{k}$-vectors that are inclined by a small angle α against the resonator axis (Fig. 8.20). The path length between the two mirrors is

$$s = d + (\lambda/2)(m^2 + n^2)^{1/2} \, . \qquad (8.23a)$$

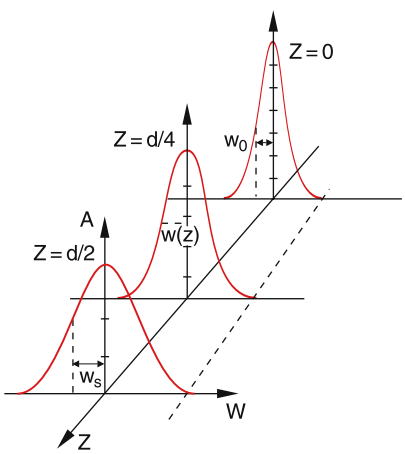

Fig. 8.19. Radial intensity profiles $I(r, z)$ and beam waists $w_s(z)$ in a confocal resonator

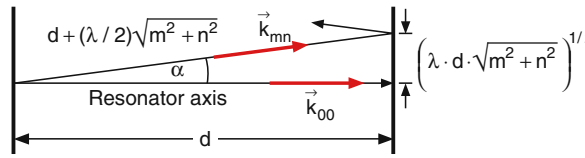

Fig. 8.20. Direction of the wave vector $\boldsymbol{k}_{mn}$ of a transverse mode $\mathrm{TEM}_{m,n,q}$ against the resonator axis

The inclination angle is

$$\tan\alpha = \left[(\lambda/d) \cdot (m^2 + n^2)^{1/2}\right]^{1/2} \, . \qquad (8.23b)$$

EXAMPLE

$d = 50\,\mathrm{cm}$, $\lambda = 500\,\mathrm{nm}$, $m = n = 1 \Rightarrow \tan\alpha = 1.2 \times 10^{-3} \Rightarrow \alpha = 0.07^\circ = 4.2'$.

Resonators with plane mirrors are often not the best choice for two reasons. They have large diffraction losses and they are very critical regarding alignment. A tilt by an angle ε changes the direction of the reflected beam by 2ε, and the reflected beam might not pass back through the active medium (Fig. 8.21a).

EXAMPLE

$d = 1\,\mathrm{m}$ and $a = 2\,\mathrm{mm}$. If the laser beam should pass 50 times through the active medium, the deviation from the correct alignment of the mirrors should not be larger than

$\varepsilon = 2 \times 10^{-3}/50 = 4 \times 10^{-5}\,\mathrm{rad} = \left(2.4 \times 10^{-3}\right)^\circ = 8.5''$.

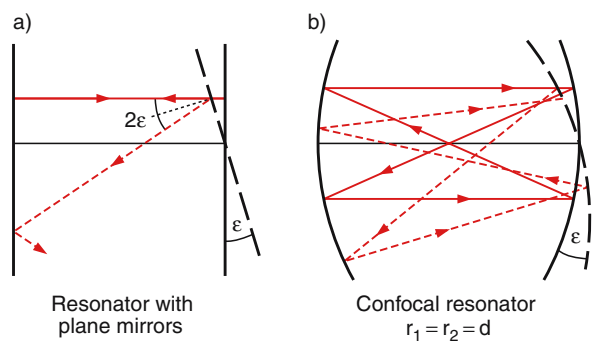

Fig. 8.21a,b. Different sensitivities against misalignment for resonators with plane mirrors (**a**) compared to confocal resonators with curved mirrors (**b**)

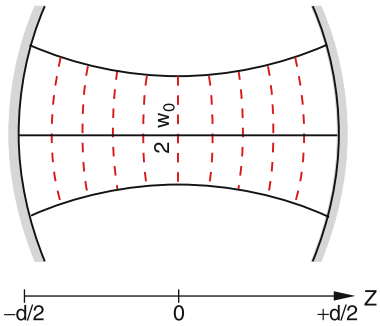

Fig. 8.22. Phase fronts at different locations z in a confocal resonator with the mirrors at $z = \pm d/2$

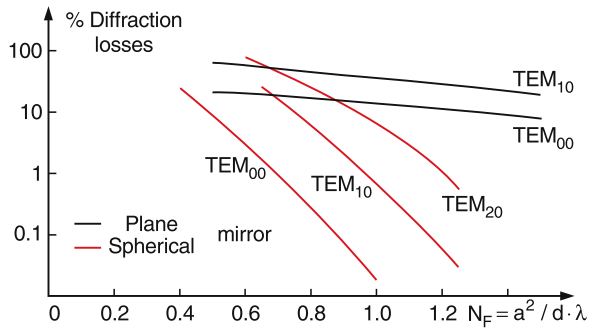

Fig. 8.23. Diffraction losses of some modes in resonators with plane and with curved confocal mirrors, as a function of the Fresnel number F

Spherical mirrors are less critical with respect to alignment, as is shown in Fig. 8.21b for the example of a confocal resonator, where the mirrors with radius of curvature r are separated by the distance $d = r$. The focal points of both mirrors coincide.

Resonators with spherical mirrors have lower diffraction losses, because they refocus the divergent diffracted beam and therefore decrease the beam spot size on the mirrors, if their radius of curvature r and their distance d is chosen properly.

In Fig. 8.19 the beam profile for the fundamental modes are shown for a confocal resonator with two spherical mirrors with equal radii of curvature r. The smallest spot size appears in the middle of the resonator at $z = 0$ when the mirrors are at $z = \pm d/2$. In Fig. 8.22 the phase fronts of the fundamental mode in a confocal resonator are illustrated. At $z = 0$ in the middle of the resonator they are plane, at the mirrors they coincide with the mirror surfaces.

8.2.4 Diffraction Losses of Open Resonators

The diffraction losses of a standing wave inside a resonator depend on the radial intensity distribution $I(r)$. The larger the intensity at the edges of the mirrors or of limiting apertures inside the resonator, the larger are the diffraction losses. This implies, that the fundamental modes TEM_{00q} have the lowest diffraction losses while the higher transverse modes with $n, m > 0$ suffer larger losses. In Fig. 8.23 the diffraction losses for the fundamental and for some transverse modes are plotted as a function of the Fresnel number N_F for resonators with plane mirrors and for confocal resonators with curved mirrors. This illustrates that for confocal resonators diffraction losses are much lower. In fact, a He-Ne-laser can only operate with curved mirrors, because otherwise the diffraction losses would be too high for the small gain achievable in a discharge with only 10–15 cm length.

These diffraction losses offer the possibility to eliminate higher transverse modes and to achieve laser oscillation solely on fundamental modes. The resonator configuration has to be chosen in such a way, that the transverse modes suffer sufficiently high losses, to prevent them from reaching the oscillation threshold.

EXAMPLE

When the gain of the active medium per roundtrip is 10% ($G(\nu) = 1.1$ in (8.3), the Fresnel number of a confocal resonator has to be $N_\mathrm{F} < 0.8$, according to Fig. 8.23, in order to prevent all transverse modes from oscillation. For a wavelength $\lambda = 600\,\mathrm{nm}$ and a mirror separation $d = 50\,\mathrm{cm}$ the limiting aperture must have a diameter of $2a = 2(N_\mathrm{F}\lambda d)^{1/2} < 10^{-4}\,\mathrm{m} \approx 1\,\mathrm{mm}$.

8.2.5 The Frequency Spectrum of Optical Resonators

For the fundamental modes with $m = n = 0$ a standing wave can build up in a resonator with plane mirrors if an integer multiple of the half-wavelength fits between the mirrors:

$$d = q\lambda/2 \Rightarrow \nu_\mathrm{r} = qc/(2d)\,. \tag{8.24a}$$

The resonance frequencies ν_r of neighboring fundamental modes are separated by

$$\delta\nu_\mathrm{r} = \nu_\mathrm{r}(q) - \nu_\mathrm{r}(q-1) = c/(2d)\,. \tag{8.24b}$$

The spacing $\delta\nu_r$ is called the ***free spectral range*** of the resonantor.

For the transverse modes TEM_{nmq} the resonance frequencies are obtained from the solutions of the integral equation (8.20), which can be solved analytically for the confocal resonator [8.9]. One obtains

$$\nu_r = \frac{c}{2d}\left(q + \tfrac{1}{2}(m+n+1)\right) , \qquad (8.24c)$$

which converts to (8.24a) for $m = n = 0$, if q is replaced by $q^* = q + \frac{1}{2}$. When $m+n$ is an odd integer, the eigenfrequencies of the transverse modes are just in the mid between two fundamental (also called longitudinal) modes.

Standing TEM_{nmq} waves with these eigenfrequencies have minimum losses. They are stored inside the resonator for a much longer time then waves with non-resonant frequencies. The total losses can be described by the sum

$$\gamma = \gamma_r + \gamma_{sc} + \gamma_{diffr}$$

of the loss factors for reflection losses, scattering and diffraction losses, where γ_{diffr} sharply increases with m and n.

The threshold condition

$$-2\alpha(\nu)L - \gamma(\nu) > 0$$

is only fulfilled for those resonance frequencies which lie within the spectral gain profile of the amplifying transition of the active medium (Fig. 8.24). The laser emission consists of all these frequencies and the total bandwidth of the laser emission depends on the width of the gain profile above the threshold line $-2\alpha L = \gamma$ in Fig. 8.24.

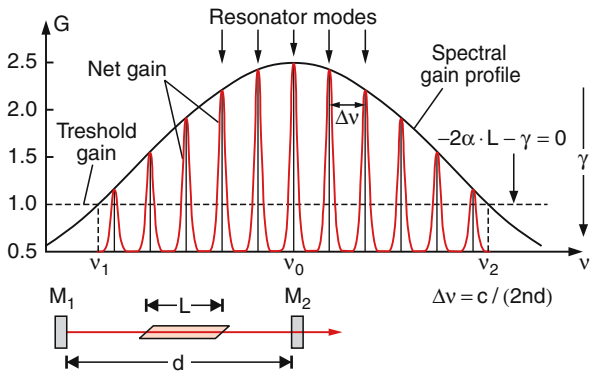

Fig. 8.24. Net gain $G(\nu)$ for resonator modes within the gain profile of the active medium. The vertical black lines give the frequencies of a multimode laser oscillating only on fundamental modes $TEM_{0,0,q}$

EXAMPLES

1. ***He-Ne Laser***: $d = 50\,\text{cm} \Rightarrow \delta\nu_r = c/2d = 300\,\text{MHz}$. Within the gainprofile with $\Delta\nu_D = 1.5\,\text{GHz}$ are Five longitudinal modes. If the discharge tube diameter is $2a < 1\,\text{mm}$, the diffraction losses are too high for transverse modes and the laser oscillates solely on these five fundamental modes.
2. ***Ruby laser***: $d = 10\,\text{cm} \Rightarrow \delta\nu_r = 1.5\,\text{GHz}$. With $2a = 6\,\text{mm}$ the diffraction losses are smaller than the high gain even for higher transverse modes. The width of the gain profile is about 30 GHz. This means that besides about 20 fundamental modes many transverse modes are present in the emission of the ruby laser.

8.3 Single Mode Lasers

In order to achieve laser oscillation on a single fundamental mode several measures can be taken.

The simplest one is the shortening of the resonator length d below a value where the mode spacing $\delta\nu_r = c/(2d)$ becomes larger than one-half of the spectral width of the gain profile at the threshold line. This, however, generally reduces the gain for gas lasers and only small output powers can be achieved. For solid state lasers with a large gain per centimeter, this might be a solution, but the spectral gain profile of these lasers is generally very broad and even short cavities still might result in multimode operation.

The better, and most commonly used method for achieving single mode operation is the insertion of additional frequency selective optical elements into the laser resonator. Such an element can be, for instance, a tiltable plane parallel glass plate with reflecting surfaces on both sides (Fig. 8.25a), which represents a Fabry-Perot etalon. As shown in textbooks on optics, the transmission of this etalon with reflectivity R on both sides is given by

$$T = \frac{1}{1 + F \cdot \sin^2(\delta/2)} \qquad (8.25)$$

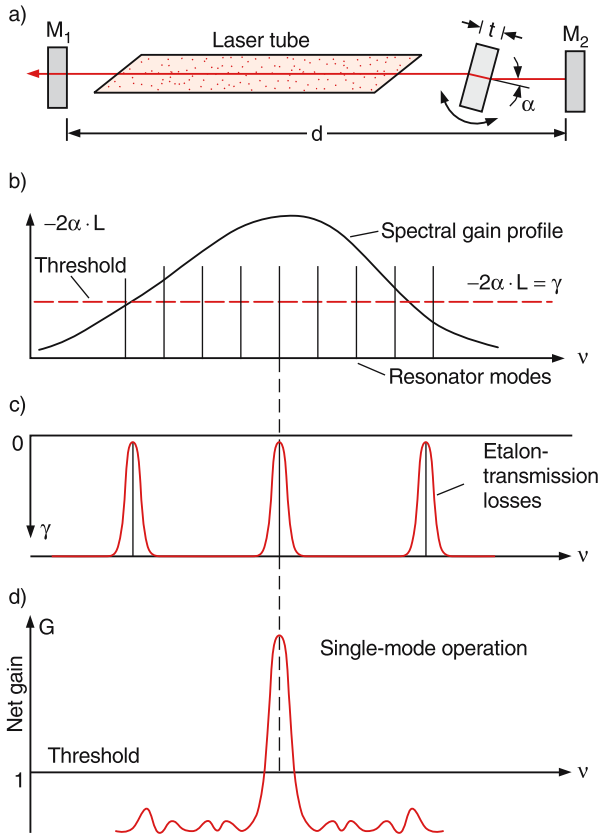

Fig. 8.25a–d. Selection of a single resonator mode (**a**) Experimental setup (**b**) Resonator modes within the gain profile of the active medium (**c**) Transmission $T(\nu)$ of the etalon (**d**) Net gain of the laser with the etalon inside the resonator

with

$$F = \frac{4R}{(1-R)^2} .$$

The phase shift $\delta = 2\pi\Delta s/\lambda$ between two adjacent interfering partial beams with angles of incidence α against the normal to the plate surfaces (Fig. 8.26) is determined by the optical path difference

$$\Delta s = 2t\sqrt{n^2 - \sin^2\alpha} . \qquad (8.26)$$

From (8.25) it follows that $T = 1$ for $\delta = 2m \cdot \pi$. This is fulfilled for all wavelengths $\lambda_m = \Delta s/m$ i.e. for all frequencies $\nu_m = c/\lambda_m = (c/\Delta s) \cdot m$, $m = 1, 2, 3, \ldots$.

Adjusting the tilting angle α correctly, one of the frequencies ν_m can coincide with a resonator eigenfrequency inside the gain profile (Fig. 8.25c). Only for this frequency are the total losses small, for all other resonator eigenfrequencies the transmission of the etalon is small and if the reflectivity R of the etalon is sufficiently high the total losses for these frequencies are larger than the gain and they do not reach oscillation threshold (Fig. 8.25d). The laser then oscillates on a single fundamental mode if the transverse modes are eliminated by high diffraction losses.

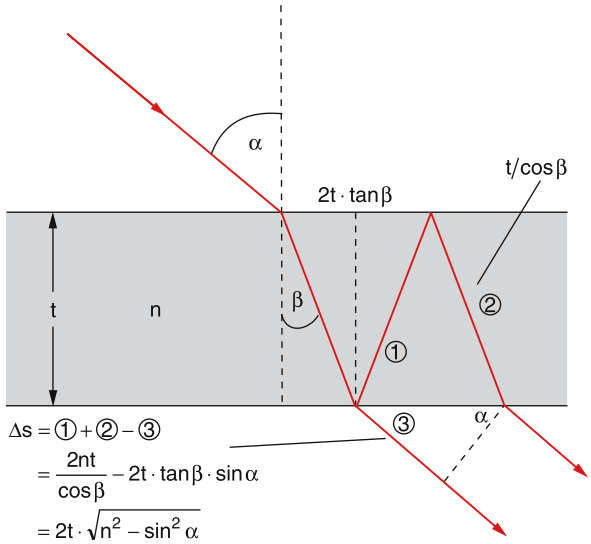

Fig. 8.26. Path difference in a plane parallel glas plate

The mean line width of such a single mode laser is mainly determined by technical fluctuations of the optical resonator length $n \cdot d$, where n is the refractive index between the resonator mirrors. Since the laser frequency is given by the eigenfrequency of the resonator

$$\nu_L = \nu_r = q \cdot c/(2nd)$$

fluctuations Δn of the refractive index or Δd of the resonator length result in corrsponding fluctuations of the laser frequency

$$\frac{-\Delta\nu_L}{\nu_L} = \frac{\Delta n}{n} + \frac{\Delta d}{d} . \qquad (8.27)$$

EXAMPLES

1. If the mirror separation $d = 50$ cm changes by 1 nm, this results in a relative frequency change $\Delta\nu/\nu = 2 \times 10^{-9}$. At a laser frequency of $\nu = 5 \times 10^{14}\,s^{-1}$ we obtain $\Delta\nu_L = 1$ MHz!

2. If the air pressure between the mirrors changes by 1 mbar, this results in a change $\Delta n/n = 2.5 \times 10^{-7}$ of the refractive index, which means a frequency shift of 125 MHz at $\nu = 5 \times 10^{14}\ \mathrm{s}^{-1}$

Such technical fluctuations can be partly compensated, if one of the resonator mirrors is mounted on a piezocrystal (Fig. 8.27). This consists of a material, that changes its length under an external voltage applied to its end faces. If part of the laser output is sent through a very stable Fabry-Perot (Fig. 8.28), the transmitted intensity changes when the laser frequency changes. A photodiode behind the FPI gives an output voltage that reflects this intensity change. The output is compared with a reference voltage and the difference is amplified and applied to the piezocrystal, which changes the resonator length and brings the laser frequency back to its wanted value. Such a feedback control system can stabilize the laser frequency within about 1 Hz! New very sophisticated devices can even reach a stability of 1 mHz $= 10^{-3}$ Hz.

The physical limitation to the line width of the laser is due to the following effect.

The laser emission starts with avalanches of photons induced by spontaneous emission. Since the spontaneous photons are randomly emitted, the amplitudes and phases of these avalanches are random. The total laser output consists of a superposition of such avalanches. This results in amplitude- and phase fluctuations of the laser wave. The amplitude fluctuations are compensated by a feedback mechanism of the active medium: A positive peak in the amplitude reduces the inversion and thus the amplification, while a negative deviation from the average amplitude increases the amplification. Such a feedback mechanism does not work for phase fluctuations, which lead to a finite line width (Sect. 7.4.3). A quantitative derivation gives the famous Schawlow–Townes formula [8.2] for the lower limit of the line width of a single mode laser:

$$\Delta\nu_{\mathrm{L}} = \frac{\pi h \nu_{\mathrm{L}}}{P_{\mathrm{L}}} \cdot \Delta\nu_{\mathrm{r}}^2 \,. \tag{8.28}$$

Here $\Delta\nu_{\mathrm{r}}$ is the width of a resonator resonance for an empty resonator, and P_{L} is the output power of the single mode laser. In Fig. 8.29 the resulting laser profile is plotted on a logarithmic scale, together with the Doppler-broadened background of the spontaneous emission.

The theoretical limit, which gives for $P_{\mathrm{L}} = 1$ W and $\Delta\nu_N = 1$ MHz a line width of 10^{-6} Hz has never been realized in a practical experiment due to the technical perturbations mentioned above. With normal expen-

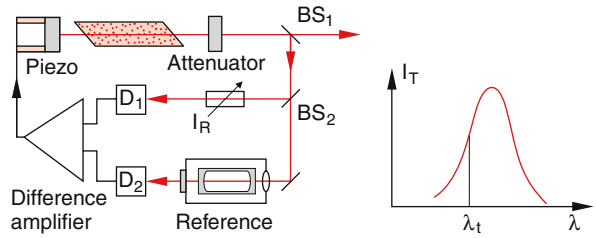

Fig. 8.28. Laser wavelength stabilization onto the slope of the transmission $T(\lambda)$ of a stable reference FPI

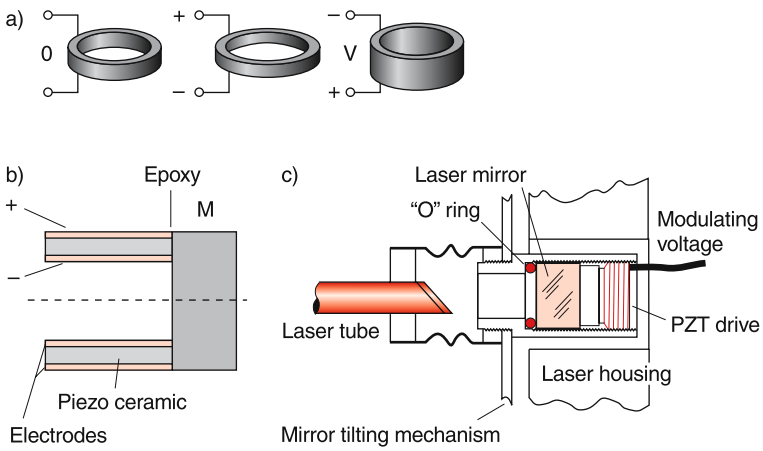

Fig. 8.27. (**a**) Piezocylinders and their (exaggerated) change of length with applied voltage (**b**) Laser mirror epoxide on a piezocylinder (**c**) Mirror plus piezomount on a single-mode tunable argon laser

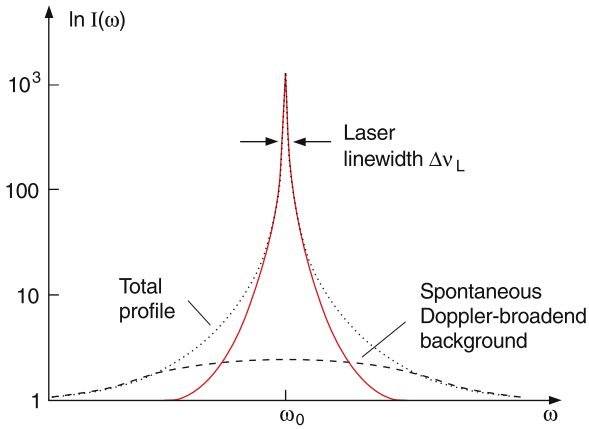

Fig. 8.29. Spectral profile of laser emission for an idealized laser without technical perturbations, plotted on a logarithmic scale

diture, a line width of about 100 kHz–1 MHz can be achieved.

Note:

A laser width a line width $\Delta\nu_L = 1$ MHz has a coherence length of $\Delta s_c = c/\Delta\nu_L = 300$ m! However, for a multimode argon laser with a bandwidth of 5 GHz the coherence length is only $\Delta\nu_c = 6$ cm, which is comparable to that of a normal discharge lamp, where a single emission line has been selected.

8.4 Different Types of Lasers

The different experimental realizations of lasers can be divided into three main groups according to their active medium:

- Solid-state lasers
- Liquid lasers
- Gas lasers

Each of these types can be operated in a pulsed mode or continuously (cw operation). Depending on the kind of energy transfer from the pump into the active medium we distinguish between optically pumped lasers (e. g., the ruby laser and other solid-state lasers, such as the neodymium laser or the titanium-sapphire laser, and the liquid-dye laser), and electrically pumped lasers (the semiconductor laser and most gas lasers pumped by an electric discharge).

Many types of lasers emit on fixed frequencies, corresponding to discrete transitions in atoms or molecules. Their wavelengths can be changed only slightly within a narrow gain profile of the atomic or molecular transition. We will call them "fixed-frequency lasers."

For spectroscopic applications "tunable lasers" are of particular importance, where the laser wavelength can be tuned over a broader spectral range. These lasers have a broad gain profile and the laser wavelength can be selected within this range by wavelength-selecting optical elements (prism, optical grating or interferometer) inside the laser resonator. Tuning the transmission peak of these elements allows a continuous tuning of the laser wavelength over the whole gain profile. Such single-mode tunable lasers represent an intense, narrow-band coherent wavelength-tunable light source, which has proved to be of invaluable advantage for numerous spectroscopic problems.

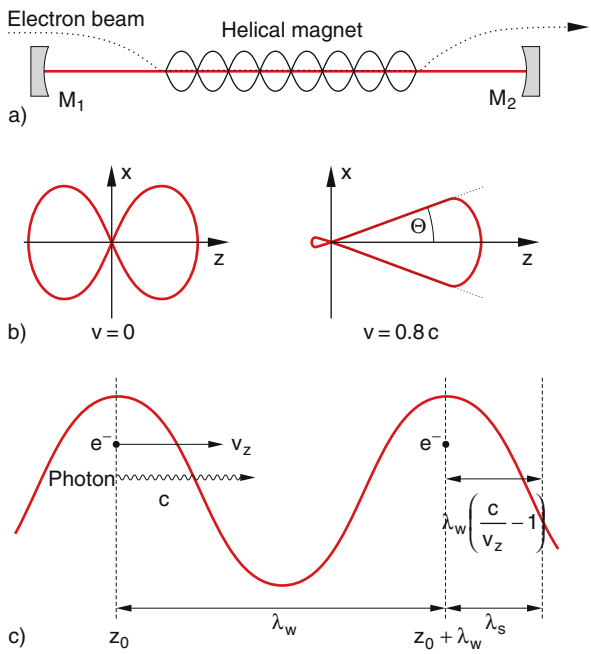

Fig. 8.30. (**a**) Schematic arrangement of a free-electron laser (**b**) Radiation of a dipole at rest ($v = 0$) and a moving dipole with $v \simeq c$ (**c**) Phase-matching condition

A completely different concept of tunable lasers uses high energy relativistic electrons from an accelerator as active medium. These electrons are forced onto oscillatory paths in a periodically changing magnetic field, where the electrons emit radiation. With a properly chosen period length of the alternating magnetic field, the contributions of the radiation from the different segments of the periodic structure superimpose in phase and add up to an intense wave in the forward direction of the average electron path (Fig. 8.30). The wavelength of the coherent emission depends on the energy of the electrons and can extend from the far infrared into the far ultraviolet. With high energy accelerators even the X-ray region can be reached. Such lasers are called ***free-electron lasers*** because their active medium consists of free electrons.

In the following sections we will discuss the most commonly used laser types.

8.4.1 Solid-state Lasers

The active medium of solid-state lasers are cylindrical rods of glass or single crystals, which are doped with special atoms, ions or molecules that can be optically pumped into excited states. The doping concentration varies between 0.1% to about 3%, depending on the kind of host material. In Table 8.1 some examples of solid-state lasers are compiled with their characteristic data.

All these solid-state lasers are optically pumped. Often pulsed flashlamps are used as pump sources, which results in a pulsed laser output. Although ruby lasers were the first lasers, these are being replaced more and more by neodymium lasers, which consist of a glass rod doped with Nd^{+++} ions emitting laser radiation at $\lambda = 1.06\,\mu m$. The advantage of the Nd lasers is based on the fact that it represents a four-level system (Fig. 8.31), which needs less inversion and therefore less pump power than the three-level ruby laser. Its infrared emission can be converted by optical frequency doubling (see Sect. 8.5) into the visible range.

The laser threshold can be further lowered by replacing the glass in the Nd-glass laser by a crystal of yttrium-aluminum-garnet (YAG), which has a higher heat conductivity and can therefore more effectively transfer the excess energy $N(h\nu_p - h\nu_L)$ (produced as heat in the rod when N photons are emitted) to the cooling system.

The pulse durations of these solid-state lasers range from microseconds to milliseconds and the output pulse

Table 8.1. Examples of solid-state lasers that can be operated in a pulsed and a cw mode

Laser type	Active Atom or Ion	Host crystal	Laser-wavelength (μm)
Ruby laser	Cr^{+++}	Al_2O_3 (Saphir)	0.6943
Neodynium-Glass-laser	Nd^{+++}	Glass	1.06
Neodynium-YAG-Laser	Nd^{+++}	$Y_3Al_5O_{12}$, CaF_2, CaF_3	1.06 0.9–1.1
Titanium-Sapphire	Ti^{+++}	Al_2O_3	0.65–1.1
Alexandrit	Cr^{+++}	$BeAl_2O_4$	0.7–0.83
Cobalt-laser	Co^{++}	MgF_2	1.5–2.1
Holmium-laser	Ho^{+++}	YAG	2.06
Erbium-laser	Er^{+++}	YAG	2.9
Colour-center laser	vacancies of alkali ions	alkali-halogenid-crystal	0.8–3.5 depending on the crystal

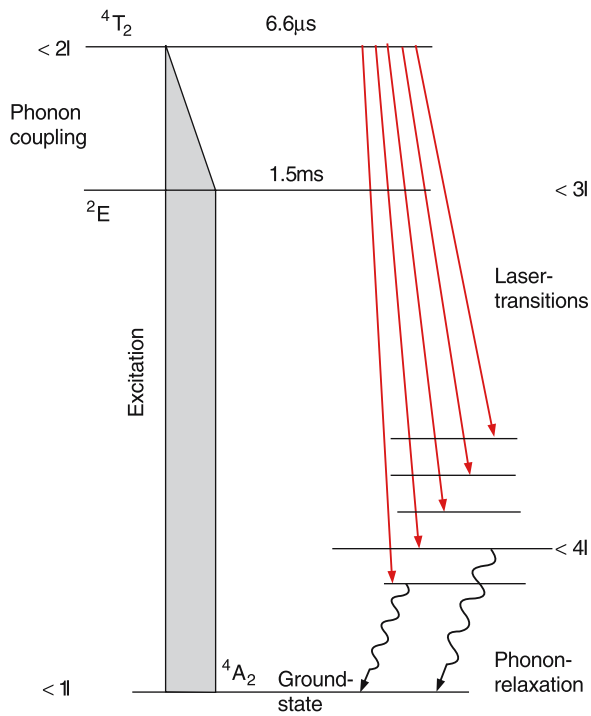

Fig. 8.31. Level scheme of the Nd:glas laser

energies from 1 mJ to about 1 J, which gives peak powers from the kW range to many MW.

In order to achieve higher output powers, the output of the laser oscillator is sent through an optical amplifier, consisting of one or several optically pumped rods, where inversion is achieved (Fig. 8.32). These laser amplifiers have a similar setup as the laser oscillator, but without the mirrors, to prevent self-starting laser oscillation in these stages. The oscillator and amplifier are separated by an optical isolator in order to prevent feedback into the oscillator.

All lasers compiled in Table 8.1 can also be pumped by continuous pump sources, e. g., with continuous lasers. They then emit cw radiation with a wavelength λ that can be tuned within the gain profile of the active medium. Some of these media have a very broad gain profile, such as the Ti:Al_2O_3 (titanium-sapphire) laser (Fig. 8.33). The reason for this broad tuning range is as follows. The optically pumped excited states relax in a very short time into a lower level, due to interactions with the vibrating atoms of the host crystal. This level represents the upper laser level. The optical transitions from this level (Fig. 8.34) can terminate on many "vibronic levels" within a low-lying electronic state, corresponding to vibrations of the host crystal Al_2O_3 (phonons). These phonons relax very fast into lower levels, thus repopulating the initial state from which the pump process starts.

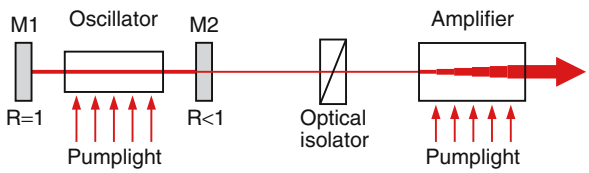

Fig. 8.32. Amplification of the laser output power by an optical amplifier

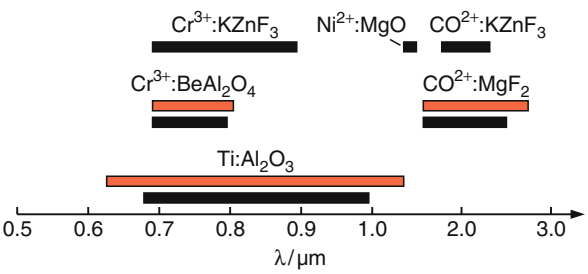

Fig. 8.33. Tuning ranges of some solid-state lasers (cw operation: *black*, pulsed operation *red*)

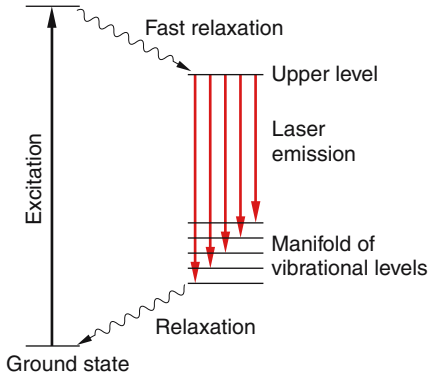

Fig. 8.34. Level scheme of vibronic solid-state lasers

Another important class of tunable solid-state lasers are color-center lasers, which consist of alkali-halide crystals (e. g., NaCl or KBr), which are transparent in the visible. If defects (a missing negative halide ion) are produced in such a crystal by X-ray irradiation, the vacancy spot acts as a potential well for the remaining electron (Fig. 8.35a). The energy levels of this electron can be excited by absorption of visible photons, thus making the crystal appear colored. Therefore these vacancies are called color centers.

When the electron is excited, the forces on the surrounding ions change. This changes their arrangements around the color center and the energy of the initially excited states $|1\rangle$ decreases to level $|k\rangle$. (Fig. 8.35b), which acts as an upper laser level. Similarly to vibronic lasers, the laser emission terminates on many vibronic levels $|i\rangle$ which relax into the initial level $|0\rangle$.

In Fig. 8.35c the tuning ranges of different color center lasers are illustrated.

8.4.2 Semiconductor Lasers

The active medium of semiconductor lasers (often called diode lasers) is a *p*-*n* semiconductor diode. An electric current is sent in the forward direction through the diode, which transports electrons from the *n*-into the *p*-section and holes from the *p*- into the *n*-section. At the *n*-*p*-junction the electrons and holes can recombine (i. e., the electrons fall from an energetically higher state in the conduction band into a lower hole state in the valence band) and may emit their recombination energy in the form of electromagnetic radiation (Fig. 8.36). The emitted radiation can be amplified when passing along the *p*-*n*-junction (stimulated recombination). Since the

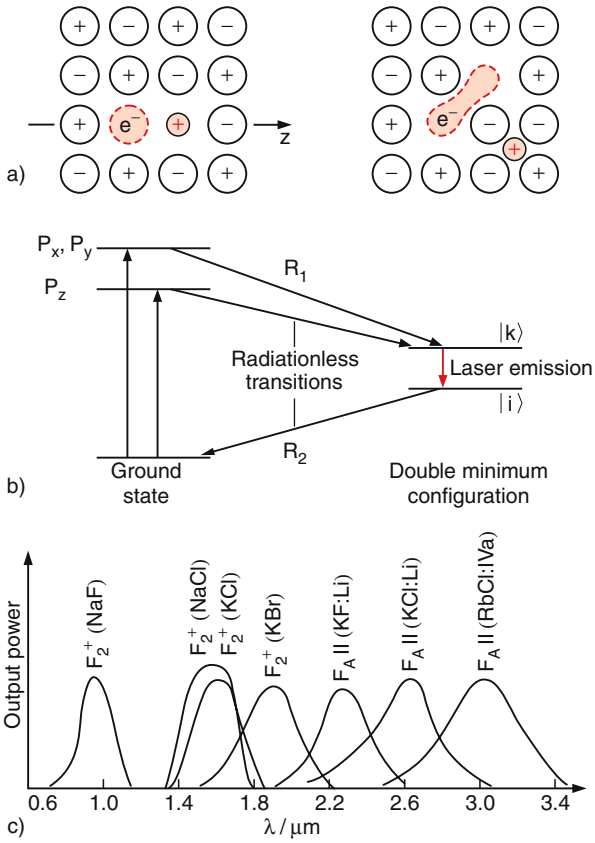

Fig. 8.35a–c. Color-center lasers. (**a**) Schematic illustration of defects in the ground state and in the relaxed upper state (**b**) Level scheme (**c**) Tuning ranges with different crystals

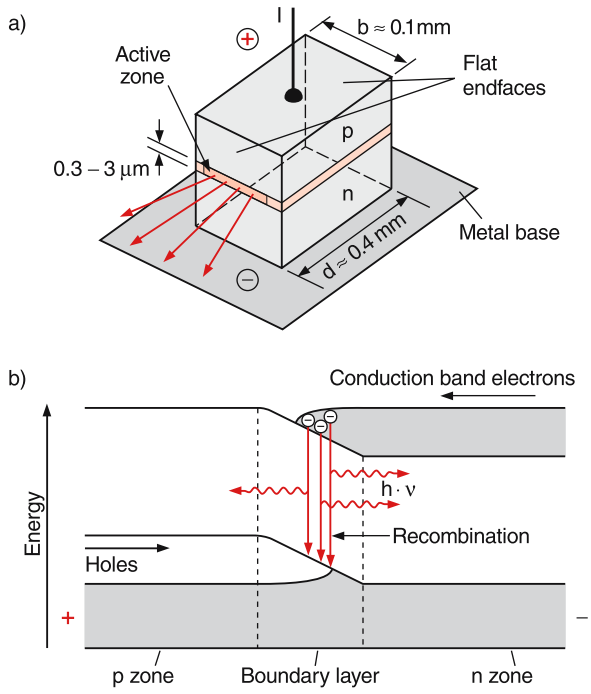

Fig. 8.36a,b. Simplified principle of a semiconductor laser. (**a**) Structure of the laser diode (**b**) Level scheme with valence and conduction band and radiative recombination of electrons with holes

electron density is very high, the amplification is correspondingly large and a path length through the active medium of less than 1 mm is sufficient to reach laser threshold.

The uncoated polished or cleaved end faces of the semiconductor crystal can serve as resonator mirrors. The refractive index of semiconductor materials is very large. For example for the GaAs (gallium-arsenide) laser emitting at $\lambda = 850\,\text{nm}$ is $n = 3.5$. The reflectivity for vertical incidence is

$$R = \left(\frac{n-1}{n+1}\right)^2 \approx 0.30\,. \tag{8.29}$$

Because of the high gain, this reflection is sufficient to surpass the laser threshold in spite of reflection losses of 0.7 per one-half roundtrip.

Typical output powers of cw semiconductor lasers are 10−50 mW, when they are pumped by an electric current of 100−300 mA. Special arrays of many simultaneously pumped diodes deliver output powers of more than 100 W! The plug-in efficiency of radiation output power to electric input power, defined as the ratio

$$\eta = P_{\text{L}}^{\text{out}} / P_{\text{el}}^{\text{in}} \approx 0.25\,,$$

reaches 25−30%, which is the highest efficiency of all lasers developed so far.

Diode lasers are more and more used for pumping other solid state lasers. Using different semiconductor materials, wide tuning ranges for the diode laser wavelengths can be achieved.

8.4.3 Dye lasers

The most important representatives of liquid lasers are dye lasers with various designs, which can be operated in a pulsed as well as in a cw mode. The active media are large dye molecules dissolved in a liquid (e. g., ethylene

glycol). These molecules have many vibration-rotation levels in the electronic ground state (singlet S_0) and in excited states (S_i or triplet states T_i). The energy level scheme is schematically depicted in Fig. 8.37. The strong interaction of the dye molecules with the liquid solvent results in a broadening of the transitions, which is larger than the average spacings between the different rotational-vibrational transitions. Instead of many discrete lines broad absorption and emission bands appear (Fig. 8.37b).

The pump source (a flashlamp or a pulsed or cw laser) excites the dye molecules from the ground state S_0 into many vibration-rotation-levels of the S_1 state. Due to the strong interaction with the solvent, the excited molecules relax within a short time (10^{-10}–10^{-12} s) into the lowest levels $|2\rangle$ of the S_1 state, from where they emit fluorescence on radiative transitions into many vibration-rotation-levels $|3\rangle$ of the S_0 state. Since these levels with energies $E > kT$ are not thermally populated at room temperature, population inversion can be reached between these levels $|2\rangle$ and the levels $|3\rangle$, if the former are sufficiently populated by optical pumping. The active medium of the dye laser is therefore a four-level system.

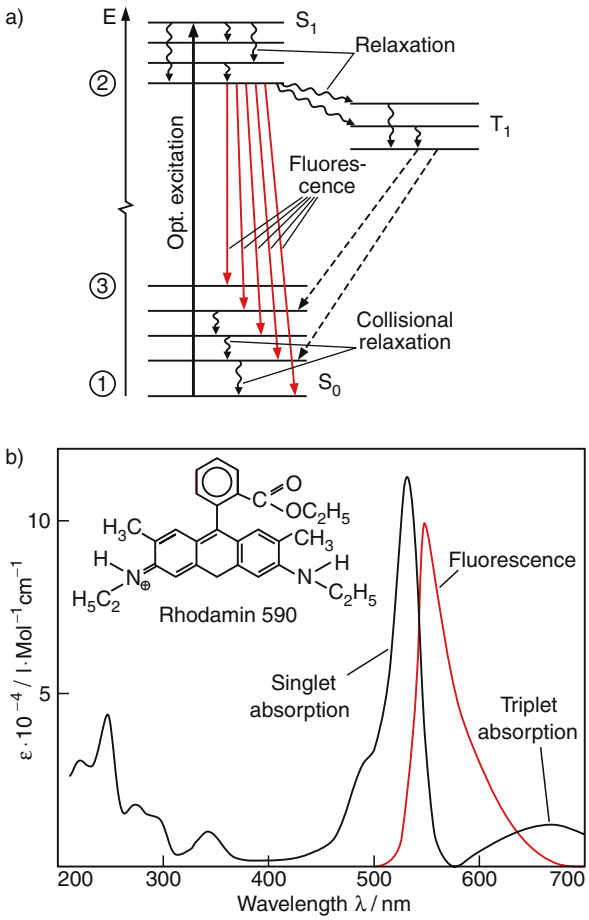

Fig. 8.37a,b. Dye laser. (**a**) Level scheme (**b**) Structure of dye molecule rhodamin 590 and absorption fluorescence spectrum

Since the absorption starts from the lower levels $|1\rangle$ and reaches higher levels in S_1 while the emission starts from the lowest levels $|2\rangle$ in S_1 and terminates on the higher levels $|3\rangle$ in S_0, the emission spectrum is red-shifted towards longer wavelengths against the absorption spectrum (Fig. 8.37b).

The dye laser can oscillate on those transitions where the threshold is reached. From the broad emission line profile a specific wavelength can be selected by wavelength-selecting elements inside the laser resonator. Tuning the transmission peaks of these elements results in a corresponding tuning of the laser wavelength. In Fig. 8.38 the tuning ranges for different dyes are shown. This figure illustrates that with different dyes the whole spectral range from 1 μm down to about 400 nm can be covered.

In Fig. 8.39 the experimental design of a flashlamp-pumped dye laser is shown. It is similar to that of the ruby laser in Fig. 8.10, but the solid rod is replaced by a glas tube through which the dye solution is pumped, producing a steady flow of dye molecules through the region pumped by the flashlamp. Because of the broad gain profile a prism is placed inside the resonator in order to select the wanted wavelength. Only that wavelength λ can oscillate, for which the laser beam hits the end mirror M_2 vertically. All other wavelengths are reflected back under an angle inclined against the resonator axis and do not reach the gain medium again. Wavelength tuning is accomplished by tilting the mirror M_2.

In Fig. 8.40 the arrangement is shown for a dye laser, pumped by another pulsed laser (e. g., a nitrogen-laser or an excimer laser (see below)). The pump beam is focused by a cylindrical lens into the dye cell, forming a line focus where inversion is achieved. The narrow dye laser beam is enlarged by telescope optics and falls onto an optical Littrow grating, where the first order diffraction is reflected back into the incident direction. This

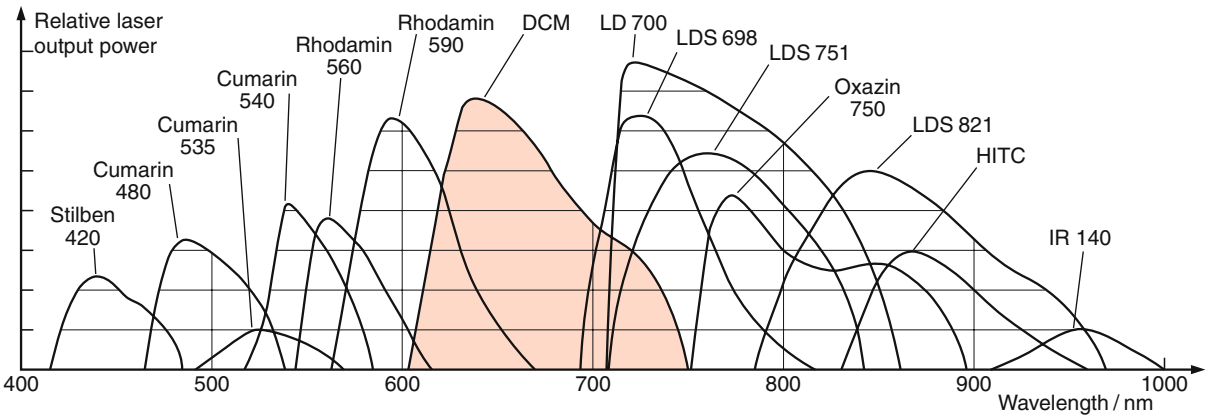

Fig. 8.38. Tuning ranges of different dyes as active medium

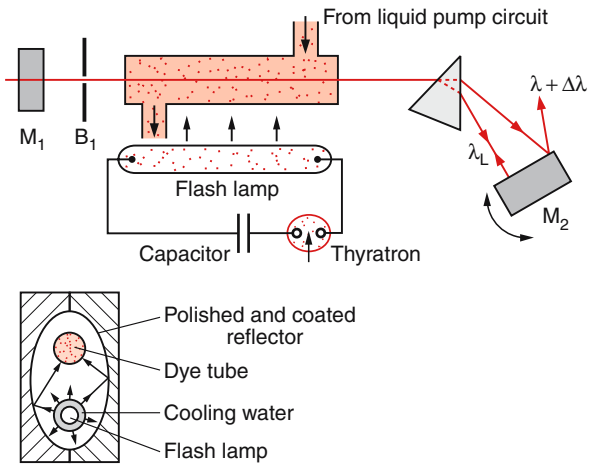

Fig. 8.39. Flashlamp-pumped dye laser

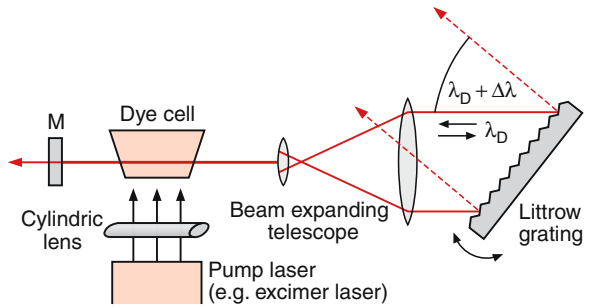

Fig. 8.40. Excimer-laser-pumped dye laser

can be realized with a grating with groove distance d, if the incidence angle α is equal to the diffraction angle β, which gives the grating equation

$$m \cdot \lambda = d(\sin\alpha + \sin\beta) = 2d \cdot \sin\alpha \qquad (8.30)$$

with $m = 1$.

The spectral resolution of the grating

$$\lambda/\Delta\lambda = m \cdot N \qquad (8.31)$$

is proportional to the number N of illuminated grooves and the diffraction order m. Therefore it is necessary to enlarge the dye laser beam to cover a large number of grooves N. Tilting the grating results in a continuous tuning of the laser wavelength.

Since the spectral width $\Delta\nu$ of pulsed lasers with pulse duration Δt is principally limited by the Fourier limitation $\Delta\nu = 1/\Delta t$, cw lasers are demanded for really high resolution in the MHz range. In Fig. 8.41 a commercial version of such a single mode cw dye laser is shown.

The active medium is a thin (≈ 0.5 mm) liquid jet of the dye solution, which is pumped by an argon laser beam, focused by a spherical mirror into the dye jet. Differently from the previously discussed resonators, four mirrors form a ring-resonator, where no standing laser wave is produced but a wave running only in one direction. This has the advantage that no nodes are present as in a standing wave and the whole inversion of the active medium can contribute to the laser amplification. In order to avoid laser waves in both directions the losses for one direction must be higher than for the other direction. This can be achieved with an optical diode (unidirectional device), consisting of a birefringent crystal and

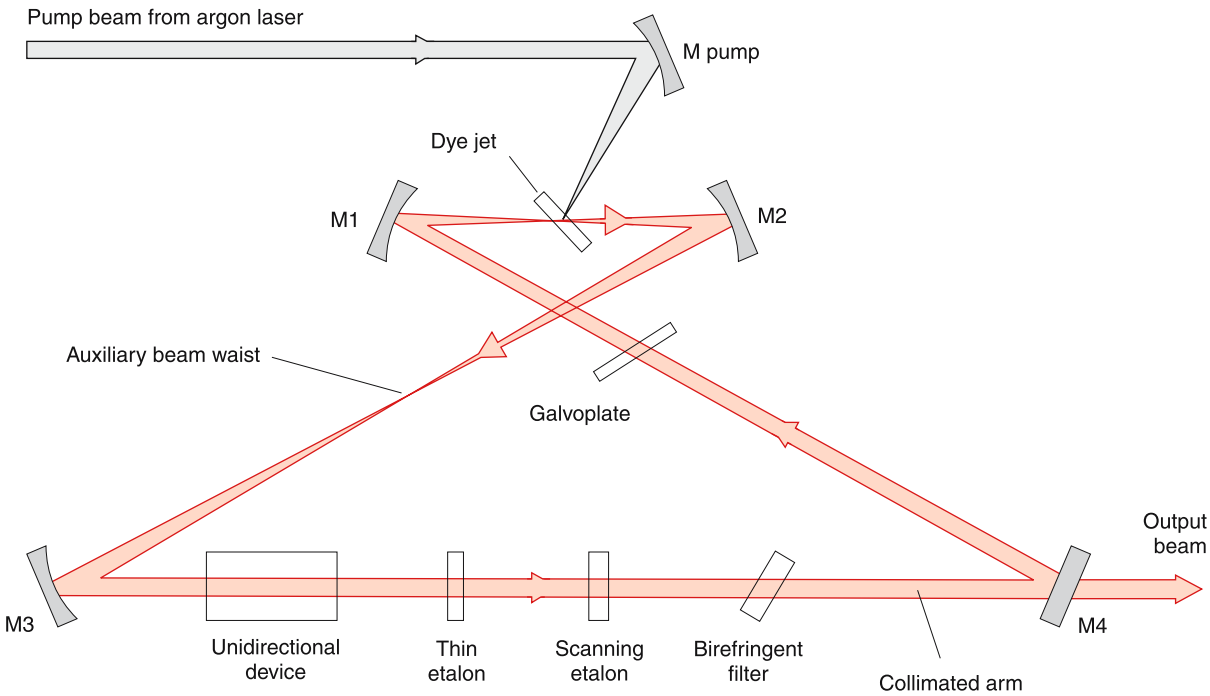

Fig. 8.41. Commercial version of a single-mode cw ring dye laser (Spectra-Physics)

a Faraday polarization rotator, which turns the birefringent rotation back to the input polarization for the wave incident in one direction, but increases the rotation for the other direction. Waves with the wrong polarization suffer large losses at the many Brewster surfaces in the resonator and therefore do not reach the threshold.

Wavelength selection is achieved with a birefringent filter and two Fabry–Perot-etalons with different thicknesses t. If the transmission peaks of all these elements are tuned to the same wavelength λ, the laser will oscillate at this wavelength as a single mode laser. The laser wavelength can be continuously tuned, if all elements and the resonator length are tuned synchronously. This can be realized with special feedback control systems. For details of these devices see [8.10].

8.4.4 Gas Lasers

Nearly all gas lasers use gas discharges as active medium. Besides the He-Ne laser already discussed in Sect. 8.1.2 the most important gas lasers are compiled in Table 8.2. Here, we will only briefly discuss the physical principles of their operation.

The ***argon laser*** oscillates on transitions between different excited levels of argon ions Ar^+. It therefore needs a high current discharge (5−50 A with 70−700 A/cm^2 current density), where the degree of ionization is high. The excitation of the upper laser levels occurs in two steps:

$$Ar + e^- \rightarrow Ar^+ + 2e^- \qquad (8.32a)$$

$$Ar^+ + e^- \rightarrow Ar^{+*}(4p, 4s) + e^- \,. \qquad (8.32b)$$

In a capillary of ceramic (length ≈ 1 m, diameter ≈ 3 mm) current densities of more than 700 A/cm^2 are reached at a total discharge current of 50 A. The gas discharge is confined by a longitudinal magnetic field in order to prevent the ions to reach the wall of the capillary where they could damage it by sputtering. The ceramic tube is cooled by a water flow between the tube and an outer cylinder on which the electric wires for the magnetic field are wound. A heated helical cathode supplies the large electron current necessary to maintain the discharge (Fig. 8.42). An elegant technical solution for the transfer of heat ($\approx$ 20−30 KW) to the cooling water is shown in Fig. 8.42b. The discharge

Table 8.2. Characteristic data of some important types of gas lasers

Laser type	Laser wavelengths	Output power
He-Ne-Laser	about 10 transitions with $\lambda = 0.54-3.39\,\mu m$	$0.1-100\,mW$
Argon laser	about 20 transitions with $\lambda = 0.35-0.53\,\mu m$	1 W–1 kW
CO_2-He-N_2-laser	about 200 transitions with $\lambda = 9.5-10.3\,\mu m$	cw: $1\,W-10\,kW$ pulsed: $\leq 1\,MW$
CO-laser	about 300 transitions $\lambda = 4.5-6\,\mu m$	cw: several watts
Excimer-laser	XeCl: 308 nm KrF: 248 nm ArF: 193 nm H_2: $150\,\mu m$	Pulse energies $1-400\,mJ/pulse$ repet. rate: $\leq 200\,Hz$
Chemical lasers	HF, DF: $2-3\,\mu m$ and $10-20\,\mu m$	several kW
Far infrared lasers pumped by CO_2-lasers	several hundred transitions with $\lambda = 50-350\,\mu m$	pulsed: mW–W

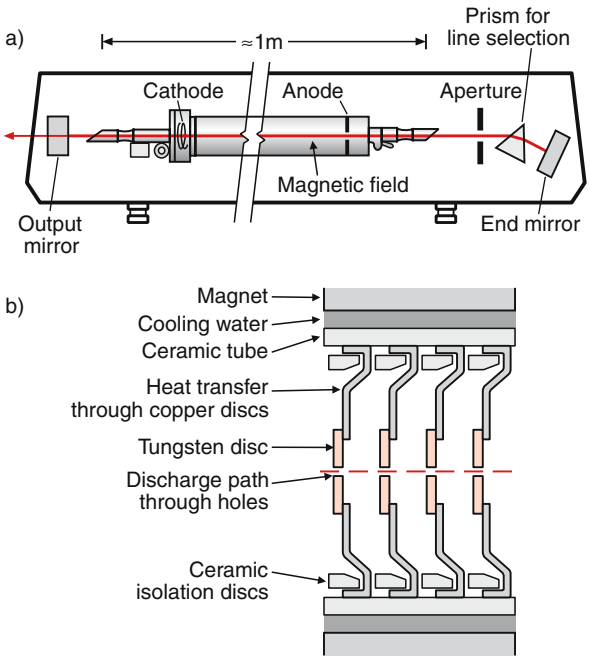

Fig. 8.42a,b. Argon ion laser. (**a**) Experimental setup (**b**) Details of the discharge path through holes drilled into tungsten discs and the heat transfer to the water-cooled envelope

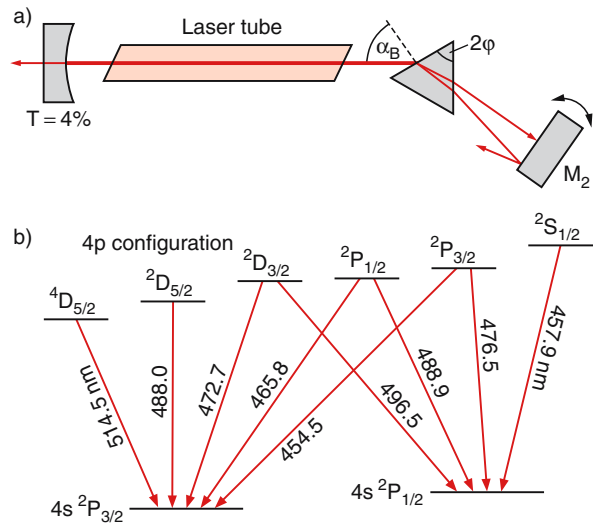

Fig. 8.43. (**a**) Laser line selection on a specific transition in argon. (**b**) Level scheme

runs through small holes (3 mm diameter) in tungsten discs, which are heated by the dissipated power to temperatures up to 1000 K. These hot discs transfer their energy by radiation to the wall of a ceramic tube with about 40 mm diameter, which is again cooled by water. The larger surface of this tube facilitates the heat transfer.

Since several upper levels in the Ar^+ ions are excited, the laser can reach oscillation threshold for several transitions and therefore oscillates on several wavelengths. A specific wavelength can be selected by a prism inside the resonator (Fig. 8.43). By tilting the mirror M_2 the desired wavelength can be chosen.

The efficiency of the argon laser

$$\eta = P_L / P_{electr} \approx 0.1\%$$

is very low. In order to produce 1 W laser output power, more than 10 kW electrical input power are necessary. Most of the power (99.9%), put into the discharge, is converted into heat transferred to the walls of the discharge and has to be taken away by the cooling water.

The ***CO_2 laser*** has the highest efficiency of all gas lasers ($\approx 10-20\%$) and for cw operation the highest output power. The active medium is a gas discharge in a mixture of He, N_2 and CO_2. By electron impact in the discharge excited vibrational levels in the electronic ground states of N_2 and CO_2 are populated (Fig. 8.44). The vibrational levels $v = 1$ in the N_2 molecule and $(\nu_1, \nu_2, \nu_3) = (00^01)$ in the CO_2 molecule (see Sect. 10.4) are near-resonant and energy transfer from the N_2 molecule to the CO_2 molecule becomes very efficient. This populates the (00^01) level in CO_2 preferentially, creates inversion between the (00^01) and the (02^00) levels, and allows laser oscillations on many rotational transitions between these two vibrational states in the wavelength range $9.6-10.6\,\mu m$. A single line can be selected by a Littrow-grating, forming one of the resonator end mirrors.

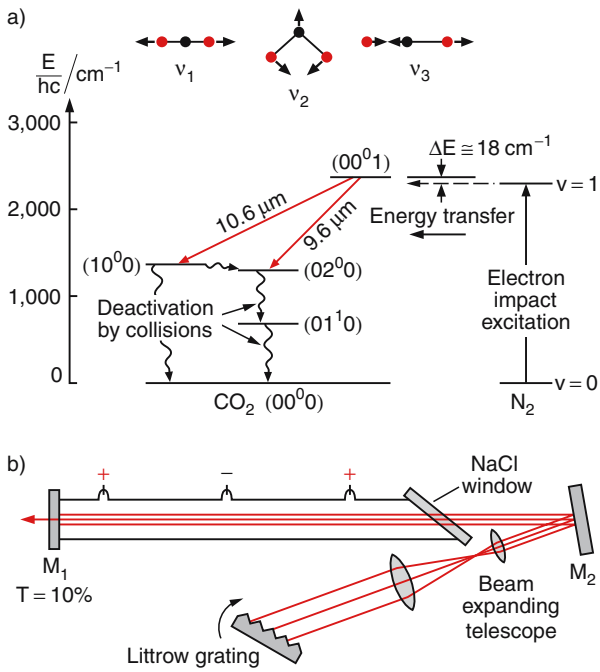

Fig. 8.44. (**a**) Level scheme and the three normal vibrational modes of the CO_2 molecule. (**b**) CO_2 laser with a Littrow-grating for line selection

Note:

The linear CO_2 molecule has three normal modes of vibration, labeled ν_1, ν_2 and ν_3, and depicted in the upper part of Fig. 8.44a (see also Sect. 10.3). The vibrational state of the molecule is described by the number of vibrational quanta in these modes. A state with 1 quantum in ν_1, 2 quanta in ν_2 and 0 quanta in ν_3 is labeled as (120). The bending vibrational mode is twofold degenerate and can have a vibrational angular momentum along the CO_2 axis. The number of quanta nh of this vibrational angular momentum is stated as an upper index to the vibrational ν_2 quanta. The upper laser level (00^01) has zero vibrational angular momentum and 1 vibrational quantum in the ν_3 mode.

A powerful gas laser in the UV is the ***excimer laser***, where specific diatomic molecules, called excimers, form the active medium. These excimers (excited dimers), are stable in an electronically excited state but unstable in their ground state (Fig. 8.45). Examples are the noble gas halides, such as XeCL, KrCL or ArF. If the stable upper state AB^* of the excimer AB is populated, (e. g., by electron excitation of the atom A and recombination $A^* + B \rightarrow (AB^*)$, inversion is automatically produced because the lower state is always completely emptied by fast dissociation on a time scale of 10^{-13} s, if it is populated by fluorescence from the upper level.

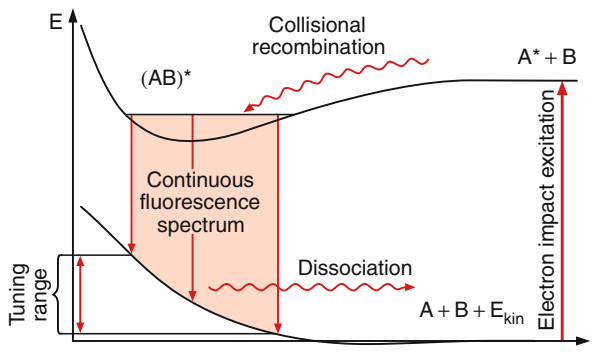

Fig. 8.45. Potential curves and fluorescence transitions of an excimer

Excimers are therefore ideal candidates for an active laser medium. They have the additional advantage that the emission from the bound upper level terminates on a repulsive potential curve on the dissociative ground state and therefore forms a broad emission continuum. This results in a broad gain profile and the wavelength of the excimer laser can be tuned over a relatively large range.

8.5 Nonlinear Optics

The optical frequency of lasers can be doubled in nonlinear optical crystals, thus considerably extending the wavelength range where coherent radiation can be generated. In this section we will briefly discuss the physical principles of optical frequency doubling or mixing under the heading nonlinear optics.

When an optical wave passes through a crystal, it induces the atomic electrons to forced oscillations. For sufficiently small electric field amplitudes $\boldsymbol{E}$ of the wave the elongations of the oscillating electrons are small and the restoring forces are proportional to the elongation (linear range). The induced dipole moments $\boldsymbol{p} = \alpha \cdot \boldsymbol{E}$ are proportional to the field amplitude and the components P_i of the dielectric polarization of the medium induced by the light wave

$$P_i = \varepsilon_0 \sum_j \chi_{ij} E_j \quad (i, j = x, y, z) \tag{8.33}$$

are linearly dependent on E, where χ_{ij} are the components of the tensor χ of the electric susceptibility. This is the realm of linear optics.

EXAMPLE

The field amplitude of the sunlight reaching the earth at $\lambda = 500\,\text{nm}$ within a bandwidth of 1 nm is about $E \approx 3\,\text{V/m}$. On the other side the electric field from the Coulomb force, binding the electron to the nucleus is, for a binding energy of 10 eV, about

$$E_\text{B} = -\frac{10\,\text{V}}{10^{-10}\,\text{m}} = 10^{11}\,\text{V/m}\,. \tag{8.34}$$

Therefore, the elongation of the electrons induced by the sunlight (for example, for the Rayleigh scattering) is very small compared with its mean distance from the nucleus and the restoring force within this small elongation is linear to a good approximation.

For much larger light intensities, as can be realized with focused beams of lasers, the nonlinear range of electron elongations can be readily reached. Instead of (8.33) the dielectric polarization has to be written as the expansion

$$\begin{aligned} P_i = \varepsilon_0 \Bigg[& \sum_j \chi_{ij}^{(1)} E_j \\ & + \sum_j \sum_k \chi_{ijk}^{(2)} E_j E_k \\ & + \sum_j \sum_k \sum_l \chi_{ijkl}^{(3)} E_j E_k E_l + \ldots \Bigg] \end{aligned} \tag{8.35}$$

where $\chi^{(n)}$ is the nth order susceptibility, which is represented by a tensor of rank $(n+1)$. The quantities $\chi^{(n)}$ decrease rapidly with increasing n. However, for sufficiently high field amplitudes E the higher order terms in (8.35) can be no longer neglected. They form the basis of nonlinear optical phenomena.

When a monochromatic light wave

$$E = E_0 \cos(\omega t - kz) \tag{8.36}$$

passes through the medium, the frequency spectrum of the induced polarization P also contains (because of the higher powers n of the field amplitudes E^n), besides the fundamental frequency ω, higher harmonics $m\omega$ $(m = 2, 3, 4 \ldots)$. This implies: The induced oscillating dipoles emit radiation not only on the frequency ω (Rayleigh scattering), but also on higher harmonics (Fig. 8.46). The amplitudes $A(m\omega)$ of these emitted waves depends on the magnitude of the coefficients $\chi^{(n)}$

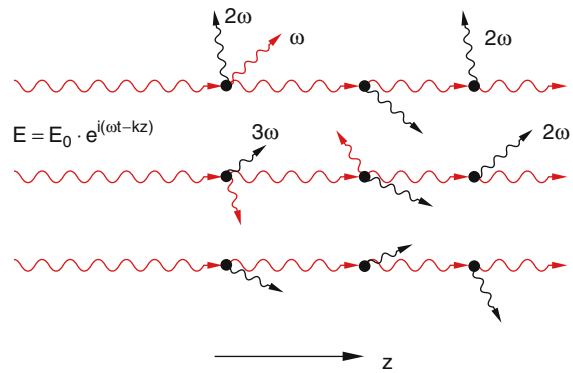

Fig. 8.46. Schematic illustration of the generation of optical harmonies under the influence of a strong electromagnetic wave

and in a nonlinear way on the amplitude E_0 of the incident light wave.

8.5.1 Optical Frequency Doubling

If the light wave (8.36) passes through an isotropic medium we obtain from (8.35), for the location $z = 0$, the x-component of the dielectric polarization

$$P_x = \varepsilon \left(\chi_{xx}^{(1)} E_{0x} \cos \omega t + \chi_{xxx}^{(2)} E_{0x}^2 \cos^2 \omega t + \dots \right) \tag{8.37}$$

when we neglect all higher order terms $\chi^{(n)}$ with $n > 2$. Similar equations are obtained for the y- and z-components. Using the relation $\cos^2 x = \frac{1}{2}(1 + \cos 2x)$ we can write (8.37) as

$$P_x = \varepsilon_0 \left(\tfrac{1}{2} \chi^{(2)} E_{0x}^2 + \chi^{(1)} E_{0x} \cos \omega t + \tfrac{1}{2} \chi^{(2)} E_{0x}^2 \cos 2\omega t \right) . \tag{8.38}$$

The dielectric polarization contains a constant term $\frac{1}{2}\varepsilon_0 \chi^{(2)} E_{0x}^2$, a linear term with frequency ω and the nonlinear term with 2ω. This means that each of the atoms hit by the incident wave radiates a scattered wave that contains the frequency ω (Rayleigh scattering) and a second harmonic wave with the frequency 2ω.

The amplitude of the second harmonic wave is proportional to the square of the amplitude of the incident wave. This means that the intensity $I(2\omega)$ is also proportional to $I^2(\omega)$.

The microscopic second harmonic waves, emitted by the different atoms, can only add up to a macroscopic wave if they are all in phase for all location in the crystal. Since the phase velocity generally depends on the frequency (dispersion), special crystals have to be used in order to match the velocities of the fundamental and the second harmonic wave.

8.5.2 Phase Matching

When a plane wave (8.36) passes through the crystal, it generates in each plane $z = z_0$ dipoles with oscillation phases that depend on the phase of the inducing fundamental wave at $z = z_0$. In a neighboring plane, $z = z_0 + \Delta z$, the same phase difference exists between the incident wave and the induced dipoles.

The waves at frequency ω, radiated by the atoms in the plane $z = z_0$ reach the next plane $z = z_0 + \Delta z$ after the same time interval as the incident wave. They therefore superimpose the microscopic waves emitted from atoms in that plane in phase and add up to twice their individual amplitude.

This is, however, not true for the second harmonic waves, because their phase velocity $v_{\mathrm{ph}}(2\omega) = c/n(2\omega)$ differs from that of the incident wave $v_{\mathrm{ph}}(\omega) = c/n(\omega)$ if the refractive index $n(2\omega) \neq n(\omega)$, which is generally the case. The second harmonic wave generated by atoms in the plane $z = z^0$ therefore reaches the plane $z = z_0 + \Delta z$ with another time delay than the incident wave and a phase difference arises between the microscopic second harmonic waves generated in the two planes. After a distance

$$\Delta z = (\lambda/2)/[n(\omega) - n(2\omega)] \tag{8.39}$$

the second harmonic wave generated in the plane $z = z_0$ arrives at the plane $z + \Delta z$ with the opposite phase as the second harmonic waves generated in this plane and therefore the two contributions interferes destructively (Fig. 8.47).

In summary: In isotropic homogeneous media the second harmonic waves generated in the different planes do not superimpose in phase. Summed over the whole crystal all phase differences between 0 and 2π occur and the total wave remains very small due to destructive interference of the different microscopic contributions.

A solution to this dilemma is provided by uniaxial birefringent crystals, where the incident light wave is

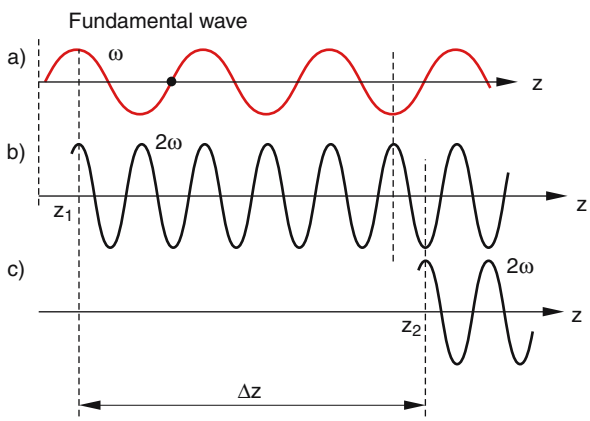

Fig. 8.47. Phase shift of π between the two harmonic waves with 2ω, generated at a point z_1 and a point $z_2 = z_1 + \Delta z$

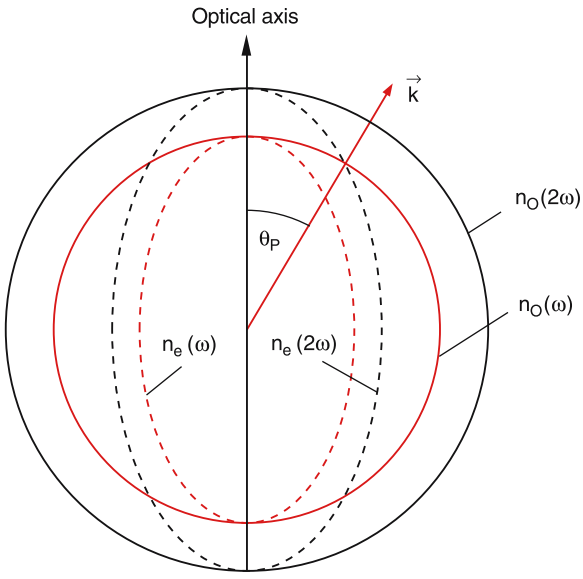

Fig. 8.48. Phase matching between fundamental wave with frequency ω and second harmonics with 2ω in birefringent optical crystals

split into an ordinary wave for which the refractive index $n = n_0$ does not depend on the direction, and an extraordinary wave where $n = n_e(\Theta)$ depends on the angle Θ between the optical axis of the crystal and the propagation direction (Fig. 8.48). At a certain angle Θ_P, called the phase matching angle, the ordinary refractive index $n_0(\omega)$ for the fundamental wave at frequency ω equals the extraordinary index $n_e(2\omega)$ for the second harmonic wave. In this direction, phase matching is possible for a selected frequency ω. The condition for phase matching can be written as

$$n_e(2\omega) = n_0(\omega) \Rightarrow v_{ph}(\omega) = v_{ph}(2\omega) \Rightarrow \boldsymbol{k}(2\omega) = 2\boldsymbol{k}(\omega)\,. \qquad (8.40)$$

If the angle Θ is changed, phase matching is achieved for another frequency ω, i. e., another wavelength λ. Therefore the phase matched wavelength can be tuned by tilting the crystal. All microscopic secondary waves at 2ω emitted into the direction Θ from the dipoles induced by the incident fundamental wave are in phase with the fundamental wave along the whole path through the crystal. Now a macroscopic second harmonic wave can build up, traveling in the same direction as the fundamental wave.

For instance, the red ruby laser emission at $\lambda = 690\,\text{nm}$ is partly converted into UV light at $\lambda = 345\,\text{nm}$ in a properly phase-matched KDP (potassium-dihydrogen phosphate) crystal. With sufficiently large nonlinear coefficients $\chi^{(2)}$ of the doubling crystal and with pulsed incident lasers of high peak powers conversion efficiencies up to $\eta = P(2\omega)/P(\omega) = 40\%$ can be achieved.

With cw lasers the output power is much less and therefore the conversion efficiency $\eta = \chi^{(2)} I(\omega)$ is smaller. One can either focus the laser beam onto the crystal to increase $I(\omega)$ at a given power $P(\omega)$, or the doubling crystal is placed inside an enhancement resonator with highly reflecting mirrors (Fig. 8.49), where the power of the fundamental wave is enhanced by a factor up to 100. With this technique a UV power of more than 50 mW can be achieved for an input power of 500 mW.

8.5.3 Optical Frequency Mixing

When two light waves

$$E_1 = E_{01}\hat{e}_x \cos(\omega_1 t - \boldsymbol{k}_1 \boldsymbol{r})$$
$$E_2 = E_{02}\hat{e}_x \cos(\omega_2 t - \boldsymbol{k}_2 \boldsymbol{r})$$

are superimposed in a nonlinear optical medium, the total electric field amplitude $E = E_1 + E_2$ induces

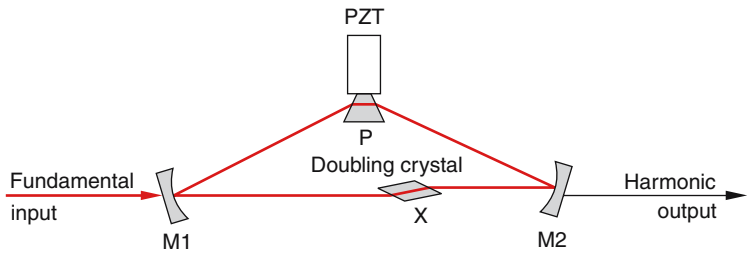

Fig. 8.49. Low-loss ring resonator with astigmatic compensation and wide tuning range for optical frequency doubling

a polarization with a nonlinear contribution

$$\begin{aligned} P^{(2)}(\omega) &= \varepsilon_0 \chi^{(2)} \big[E_{01}^2 \cos^2 \omega_1 t + E_{02}^2 \cos^2 \omega_2 t \\ &\quad + 2E_{01} E_{02} \cos \omega_1 t \cdot \cos \omega_2 t \big] \\ &= \tfrac{1}{2} \varepsilon_0 \chi^{(2)} \big[\left(E_{01}^2 + E_{02}^2 \right) \\ &\quad + \left(E_{01}^2 \cos 2\omega_1 t + E_{02}^2 \cos 2\omega_2 t \right) \\ &\quad + 2E_{01} E_{02} (\cos(\omega_1 + \omega_2) t \\ &\quad + \cos(\omega_1 - \omega_2) t) \big] . \end{aligned} \tag{8.41}$$

Besides the second harmonics at frequencies $2\omega_1$ and $2\omega_2$ also waves are generated with the sum frequency $\omega_1 + \omega_2$ and the difference frequency $\omega_1 - \omega_2$, if the phase matching condition can be properly chosen for each of these different contributions. For example, the phase-matching condition for the macroscopic generation of the sum frequency $\omega_3 = \omega_1 + \omega_2$ is

$$\boldsymbol{k}(\omega_1 + \omega_2) = \boldsymbol{k}_1(\omega_1) + \boldsymbol{k}_2(\omega_2) \Rightarrow \tag{8.42a}$$

$$n_2 \omega_3 = n_1 \omega_1 + n_2 \omega_2 \quad \text{with} \quad n_i = n(\omega_i) . \tag{8.42b}$$

This condition is generally more readily fulfilled than that for the second harmonic generation, because the directions of the two incident waves (and therefore their wave vectors) can be freely chosen within certain limits, which imposes less restrictions to the selection of the nonlinear crystal.

The possibility of optical frequency mixing has greatly increased the spectral ranges covered by intense coherent light sources. With difference-frequency generation, using two visible lasers, the mid-infrared region can be covered, while sum-frequency generation gives access to the UV range down to $\lambda = 200\,\text{nm}$. The spectral limitations are given by the spectral regions where the absorption of the nonlinear crystal becomes large.

8.6 Generation of Short Laser Pulses

The investigation of fast processes induced by the absorption of photons, demand a high time resolution of the detection technique. Examples for such fast processes are the decay of excited states with a short lifetime, the dissociation of molecules or the rearrangement of molecular structure after excitation into higher energy states. This latter process plays an important role in the visual process, where the primarily excited rhodopsin molecules in the retina of the eye undergo many energy transfer process before the excitation energy is transferred into an electrical signal reaching our brain. Such processes could only be studied in detail after the development of ultrashort laser pulses with pulse widths down to about five femtoseconds ($1\,\text{fs} = 10^{-15}\,\text{s}$).

In this section we will briefly discuss some experimental techniques for the generation of short laser pulses.

8.6.1 Q-Switched Lasers

The inversion threshold for obtaining laser oscillation depends on the total losses (see Sect. 8.1.1), which can be expressed by the quality factor (Q-factor) of the laser resonator.

The Q-value of the kth resonator mode is defined as

$$Q_k = -\frac{2\pi \nu W_k}{\mathrm{d}W_k/\mathrm{d}t} = +\frac{\omega}{\gamma_k} T_\mathrm{R} \tag{8.43}$$

and can be expressed by the total loss factor γ_k of this mode and the roundtrip time $T_\mathrm{R} = 2d/c$.

The Q-switching technique uses the following trick: During the pump process the Q-value of the laser resonator is kept so low (i.e., the losses are so high) that the laser threshold is not reached in spite of the growing inversion. At a selected time $t = t_\mathrm{s}$, Q is suddenly switched to a maximum value (Fig. 8.50). This prevents laser oscillation for $t < t_\mathrm{s}$ and allows the population inversion to reach a large value, because it is not depleted by induced emission. When the losses are suddenly switched to a minimum value at $t = t_\mathrm{s}$ the inversion is way above threshold and the amplification of the spontaneous emission starting the photon avalanche is accordingly high. This leads to a fast rising "giant

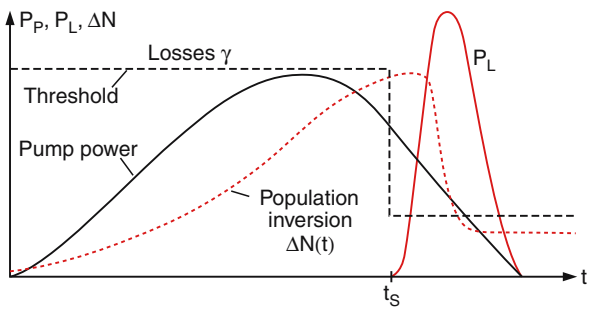

Fig. 8.50. Pump power $P_\mathrm{P}(t)$, laser output power $P_\mathrm{L}(t)$, and cavity losses $\gamma(t)$ for a Q-switched laser

pulse", which depletes the inversion within a short time and therefore terminates itself.

In Fig. 8.51 two possible experimental realizations of Q-switched lasers are shown. A fast spinning resonator mirror spoils the Q-value for all times, except for the short time span where the mirror surface is perpendicular to the resonator axis. The light from a light-emitting diode is reflected by the backside of the spinning mirror onto a photodetector. Its output signal triggers the discharge of the flashlamp, pumping the laser. An electronic delay of the trigger signal can select the time delay between trigger time and vertical position of the spinning mirror.

The optimum time delay depends on the duration of the pump pulse and on the lifetime τ of the upper laser level. The time delay must be smaller than the lifetime τ, because otherwise one looses too much of the upper state population necessary for the amplification of the giant pulse.

Another more commonly employed technique uses a Pockels cell inside the laser resonator for Q-switching. A Pockels cell consists of a birefringent crystal that changes its birefringence with an applied electric field. If the crystal is biased in such a way that it rotates the plane of polarization by 45° for one transit, the light transmitting the crystal a second time after reflection by mirror M_2 has its plane of polarization turned by 90°. A polarization beam splitter then reflects the beam out of the laser resonator (Fig. 8.51b). At the Q-switching time t_s, a high voltage pulse is suddenly applied to the crystal that changes the birefringence and brings the rotation angle per transit to 90° and for the reflected beam to 180°. The beam is now transmitted by the polarization beam splitter and reaches the laser rod.

These techniques generate giant laser pulses with durations of a few ns and peak powers of 10^5-10^9 W, depending on the laser type.

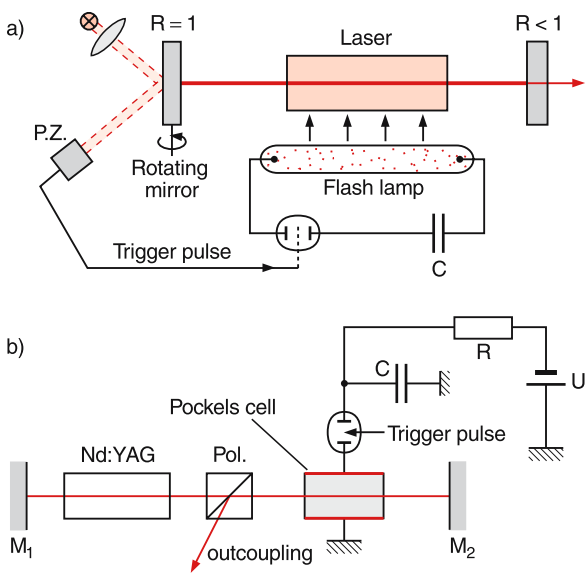

Fig. 8.51a,b. Possible realizations of cavity Q-switching (**a**) With a rotating resonator mirror (**b**) With an electro-optic switch (Pockels cell) inside the laser resonator

8.6.2 Mode-Locking of Lasers

Much shorter pulses can be achieved with the mode-locking technique, which is based on the following principle.

If a light wave with optical frequency ν_0 passes through an optical modulator with a modulation frequency f (e. g., a Pockels cell or an ultrasonic modulator), the transmitted amplitude intensity is modulated according to

$$I_t = I_0[1 + a\cos(2\pi ft)]\cos^2(2\pi\nu_0 t)\ . \qquad (8.44)$$

The degree of modulation $a < 1$ depends on the voltage applied to the modulation cell. The Fourier analysis of such a modulated light wave gives a frequency spectrum that consists of the carrier frequency ν_0 and sidebands at frequencies $\nu_0 \pm n \cdot f$.

Inserting the modulator inside the laser resonator (Fig. 8.52) and choosing the modulation frequency f to be equal to the frequency separation

$$\delta\nu = c/2d = f$$

of the longitudinal resonator modes, makes all sidebands resonant with resonator modes. This means that the sidebands can participate in laser oscillation as long as their frequencies lie within the gain profile of the active medium. This leads to a coupling of all resonator modes within the gain profile because the phases of the sidebands are coupled to that of the carrier by the phase of the modulation.

If the modulator has the time dependent transmission

$$T = T_0\left[1 - a\sin^2(\Omega/2)t\right] \qquad (8.45)$$

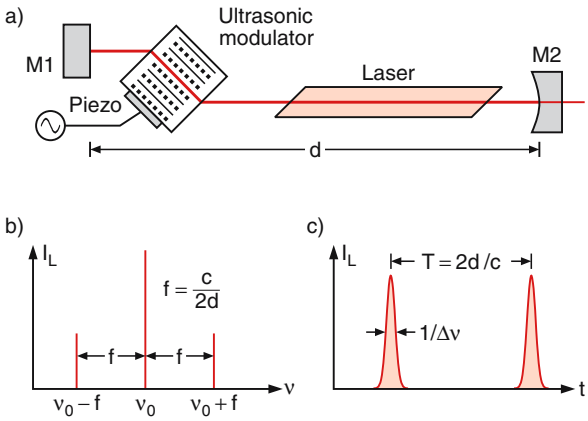

Fig. 8.52a–c. Mode-locking of lasers. (**a**) Experimental setup with an ultrasonic modulator (**b**) Laser frequency ν_0 and the two neighboring side-bands (**c**) Laser output pulses with width $\Delta t \approx 1/\Delta\nu$ and repetition frequency $f = 1/T = c/2d$

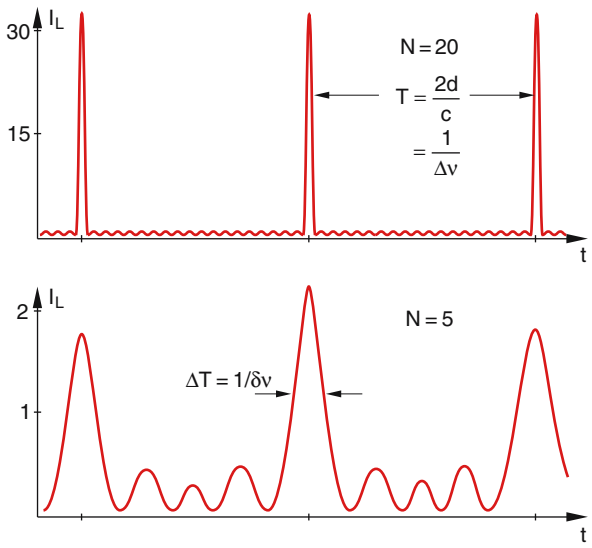

Fig. 8.53. Mode-locked pulses, where N modes have been locked. Note the different ordinate scales

with the modulation frequency $f = \Omega/2\pi$ and the modulation amplitude $a < 1$, the amplitude ot the kth mode becomes

$$A_k(t) = TA_{ki}\cos\omega_k t \qquad (8.46)$$
$$= T_0 A_{k0}\left[1 - a\sin^2(\Omega/2)t\right]\cos\omega_k t\,.$$

This can be written as

$$A_k(t) = T_0 A_{k0}\left[\left(1 - \frac{a}{2}\right)\cos\omega_k t \right. \qquad (8.47)$$
$$\left. + \frac{a}{4}\left[\cos(\omega_k + \Omega)t + \cos(\omega_k - \Omega)t\right]\right].$$

The total amplitude of $N = 2m + 1$ coupled modes is then

$$A(t) = \sum_{k=-m}^{+m} A_k \cos(\omega_k + k\cdot\Omega)t$$

For equal amplitudes $A_k = A_0$ the total time-dependent intensity becomes

$$I(t) \propto A_0^2 \frac{\sin^2\left(\frac{1}{2}N\Omega t\right)}{\sin^2\left(\frac{1}{2}\Omega t\right)}\cos^2\omega_0 t\,. \qquad (8.48)$$

For cw lasers the amplitude A_0 is constant in time and (8.48) represents an equidistant sequence of pulses (Fig. 8.53) with a pulse separation

$$T = \frac{2d}{c} = \frac{1}{\Delta\nu}\,, \qquad (8.49)$$

which equals the roundtrip time through the laser resonator. The pulse width

$$\Delta T = \frac{2\pi}{(2m+1)/\Omega} = \frac{2\pi}{N\Omega} = \frac{1}{\delta\nu} \qquad (8.50)$$

is determined by the number N of phase locked modes within the gain profile with spectral width $\delta\nu$ and is therefore inversely proportional to the spectral bandwidth $\delta\nu$ of the gain profile above threshold.

The peak power of the pulses is proportional to N^2. The pulse energy is proportional to $N^2\Delta T \propto N$. In between two succesive main pulses $(N-2)$ small maxima appear, which decrease in intensity as N increases (Fig. 8.53).

Contrary to a normal multimode laser that can oscillate simultaneously on many modes with, however, random phases, the mode-locked laser oscillates on many phase-coupled modes, because the modulator enforces a definite phase relation between the oscillating modes.

EXAMPLES

1. The gain profile of the He-Ne laser has a width of about $\Delta\nu = 2\,\text{GHz}$. Mode-locking therefore achieves pulses with a minimum duration of $\Delta\tau = 500\,\text{ps}$.

2. The argon laser has a larger spectral width $\Delta\nu = 6\,\text{GHz}$ of its gain profile and allows mode-locked pulses with widths down to $\Delta\tau = 170\,\text{ps}$.
3. The dye laser has a very large spectral bandwidth of about $\Delta\nu = 3\times10^{13}\,\text{s}^{-1}$. Therefore, pulses down to $\Delta\tau = 3\times10^{-14}\,\text{s}$ should be possible. The experimental realization only reaches $\Delta\tau = 3\times10^{-12}\,\text{s} = 3\,\text{ps}$. This corresponds to the transit time $\Delta t = \Delta x/c$ of the light through the modulator with length Δx.

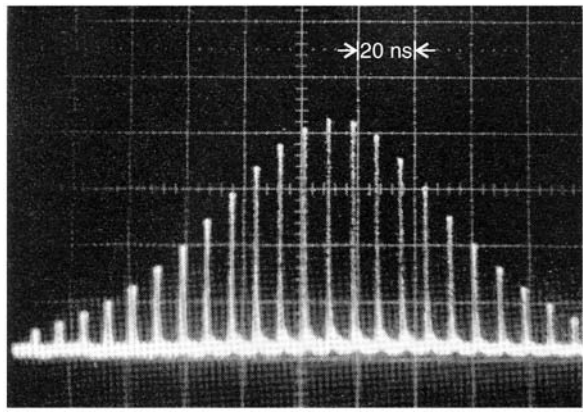

Fig. 8.54. Periodic pulse sequence from a pulsed mode-locked Nd:glass laser (W. Rudolf, F.B. Physik, Univ. Kaiserslautern)

Not only cw lasers, but also pulsed lasers, can be mode-locked. The pulse amplitude is no longer constant but follows the time profile of the gain. In Fig. 8.54 the pulse sequence within one pulse envelope of a mode-locked neodymium-glass laser is shown for illustration.

The shortest laser pulses, obtained so far are generated by a nonlinear effect, called Kerr lens mode-locking. Its basic principle is illustrated in Fig. 8.55.

For sufficiently high intensities, the refractive index is affected by the nonlinear interaction of the light wave with the medium. It can be written as a sum

$$n(\omega, I) = n_0(\omega) + n_2(\omega)\cdot I \tag{8.51}$$

where $n_0(\omega)$ is the normal refractive index and $n_2(\omega) \ll n_0(\omega)$. The intensity-dependent change of the refractive index is caused by the nonlinear polarization of the atomic electron shells induced by the electric field of the optical wave and is therefore called the optical Kerr effect.

When a laser beam with a Gaussian radial intensity profile $I(r)$ passes through a medium, the refractive index shows a radial gradient with a maximum value of n at the central axis at $r = 0$. The medium then acts like a lens and leads to a focusing of the incident laser beam, where the focal length depends on the laser intensity.

When a laser pulse with the time profile $I(t)$ passes through the medium, the central part of the pulse around its maximum generates the largest gradient of $n(r)$ and

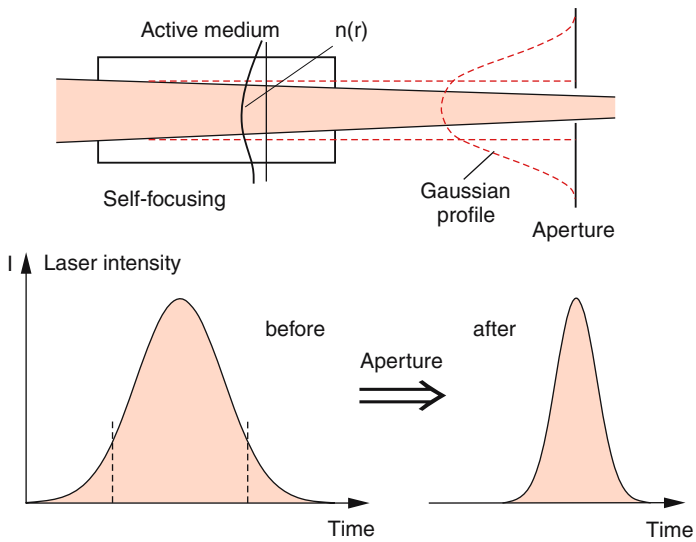

Fig. 8.55. Kerr-lens mode-locking

therefore the shortest focal length f_{min} of the Kerr lens. If an aperture is placed at a distance f_{min} behind the Kerr lens, only that part of the pulse $I(t)$ around its maximum at $t = t_0$ is fully transmitted through the aperture. All other parts before and after the maximum produce a longer focal length and therefore have a larger spot size at the aperture and only the central part of the radial beam profile is transmitted through the aperture. These parts of the pulse therefore suffer larger losses and are attenuated. This happens for every roundtrip inside the resonator and leads to a shortening of the pulse duration.

EXAMPLE

For sapphire Al_2O_3 $n_2 = 3 \times 10^{-16}\,cm^2/W$. For the intensity $I = 10^{14}\,W/cm^2$ the refractive index changes by $\Delta n = 3 \times 10^{-2}\, n_0$ with $n_0 = 1.76$. For a laser pulse with a wavelength $\lambda = 1\,\mu m$ this leads to an additional phase shift of the optical phase by $\Delta\varphi = (2\pi/\lambda)\Delta n = 2\pi \times 300 \cdot 1.76$ after a pathlength of 1 cm through the Kerr lens material, which results in a radius of curvature $R = 4\,cm$ of the wavefront of the light wave. For a Gaussian beam profile with peak intensity $I(0) = 10^{14}\,W/cm^2$ which would be a plane wave without the Kerr lens, the focal length of the Kerr lens is then $f = 4\,cm$.

This Kerr lens mode-locking has been successfully applied to the generation of ultrashort light pulses from a Ti:sapphire laser, which has a very broad gain profile and is therefore well suited to allow such short pulses. In Fig. 8.56 a possible experimental realization is shown. The Kerr medium is the Ti:sapphire crystal, which acts simultaneously as active laser medium, and the limiting aperture is placed in front of mirror M_4. The Kerr lens changes the focal length and therefore the imaging

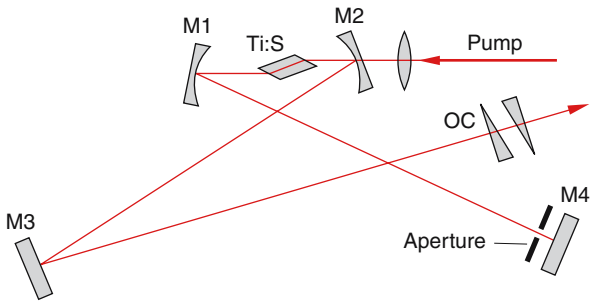

Fig. 8.56. Experimental setup for a Kerr-lens mode-locked Ti:sapphire laser (OC = optical compensator)

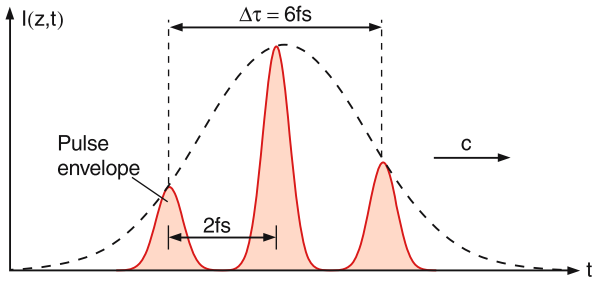

Fig. 8.57. Schematic representation of an ultrashort light pulse containing only three optical cycles of the light intensity. The envelope has a half-width of $\Delta\tau = 6\,fs$ and a spatial extension $\Delta z = c \times \Delta\tau \approx 2\,\mu m$

characteristics of the laser resonator in such a way that for the maximum of the laser pulse the focus lies in the center of the aperture.

With such a device, pulses down to 4 fs have been achieved. For these short pulses the spectral width is very large and any dispersion effects in the laser resonator must be carefully compensated for. For instance, the dielectric mirrors with many reflecting layers generally have a wavelength- dependent phase shift, which would lead to a broadening of the pulse. Therefore special dispersion-compensated mirrors have been designed that avoid this problem.

For an optical wave at $\lambda = 600\,nm$ ($\nu = 5 \times 10^{14}\,s^{-1}$), the optical cycle time is $T_{opt} = 1/\nu = 2\,fs$. A light pulse of 6 fs half-width therefore contains only three optical cycles (Fig. 8.57).

8.6.3 Optical Pulse Compression

When a short optical pulse is sent through an optical fiber with a core diameter of 5 μm, the intensity becomes so high that the refractive index

$$n(\omega) = n_0(\omega) + n_2 \times I(t)$$

is changed by the nonlinear interaction of the medium with the laser pulse. It becomes time-dependent. The nonlinear term n_2 can be positive as well as negative, depending on the material and the laser wavelength.

A short pulse of duration ΔT can be described by the wave packet

$$I(t) = \int_{-\Delta\omega/2}^{+\Delta\omega/2} I(\omega)\, e^{i(\omega t - kz)}\, d\omega\,. \qquad (8.52)$$

This represents a superposition of many frequency components within the frequency interval $\Delta\nu = 1/\Delta T = \Delta\omega/2\pi$ where $I(\omega)$ gives the envelope of the spectral profile.

The linear part $n_0(\omega)$ of the refractive index causes, for normal dispersion ($\mathrm{d}n_0/\mathrm{d}\lambda < 0$), a larger phase velocity for the red components in the pulse than for the blue components. The red components will therefore be at the leading edge and the blue components at the trailing edge of the pulse. This results in spatial- and time-broadening of the pulse.

The nonlinear part $n_2 I(t)$ causes a frequency shift dependent on the intensity. This can be seen as follows. The phase of the wave $E = E_0 \cos(\omega_0 t - kz)$

$$\varphi = \omega_0 t - kz = \omega_0 t - \omega n z/c \qquad (8.53)$$
$$= \omega_0 \cdot (t - n_0 z/c) - A \cdot I(t)\,; \quad A = n_2 \omega z/c$$

depends on $I(t)$. Since the frequency

$$\omega = \mathrm{d}\varphi/\mathrm{d}t = \omega_0 - A \cdot \mathrm{d}I/\mathrm{d}t \qquad (8.54)$$

is the time derivative of the phase φ, it is evident from (8.53) that with $A > 0$ the frequency at the leading edge of the pulse ($\mathrm{d}I/\mathrm{d}t > 0$) is decreased and at the trailing edge ($\mathrm{d}I/\mathrm{d}t < 0$) is increased. This phenomenon is called a chirp of the optical pulse, where the optical frequency changes from small to high frequencies over the pulse profile $I(t)$ (Fig. 8.58).

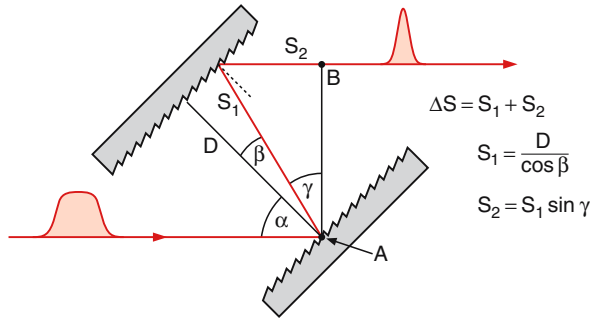

Fig. 8.59. Optical pulse compression by a grating pair

In summary, when passing through an optical medium the optical pulse $I(t)$ becomes broader, caused by the dispersion $n_0(\omega)$, and its spectral profile $I(\omega)$ becomes broader due to the chirp induced by the nonlinear part $n_2 \cdot I(t)$ of the refractive index.

When such a spectrally broadened pulse is sent through a pair of parallel optical gratings (Fig. 8.59),

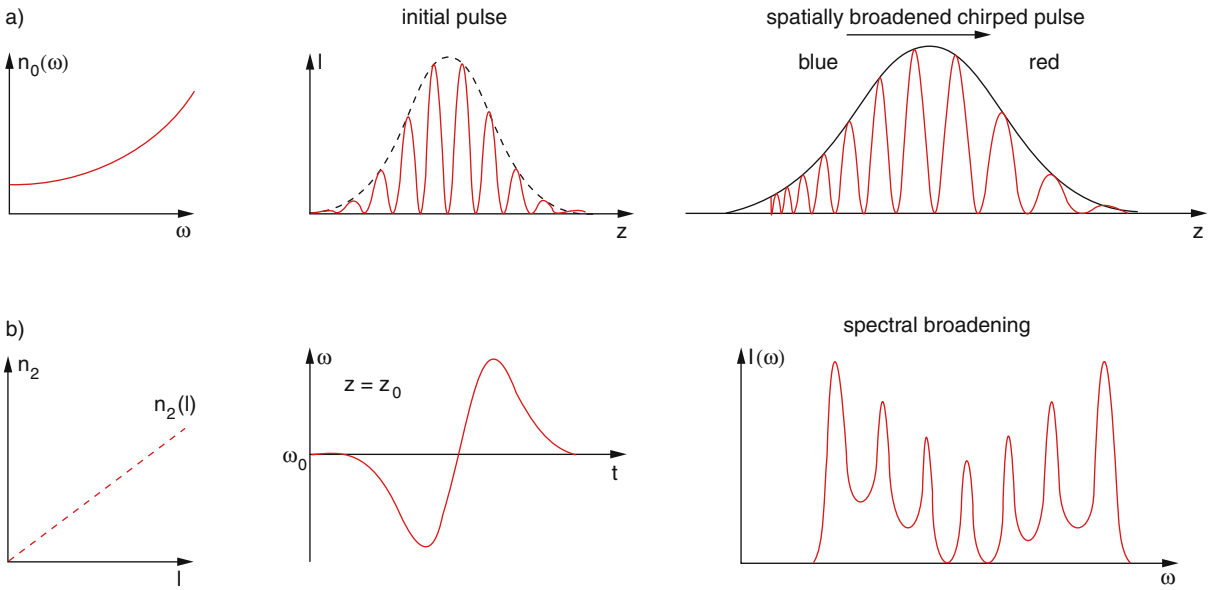

Fig. 8.58a,b. Spatial and spectral broadening of a pulse in a medium with normal linear (**a**) and nonlinear (**b**) refractive index

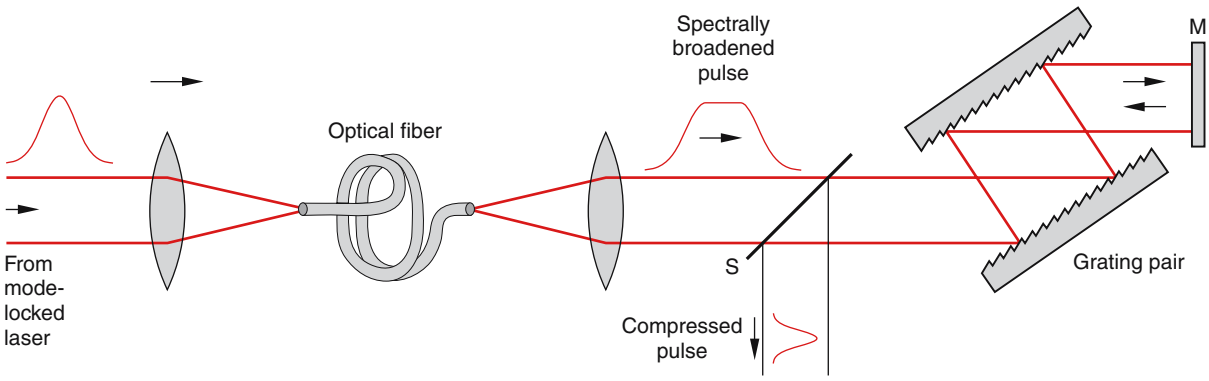

Fig. 8.60. Experimental arrangement for the generation of femtosecond pulses by self-phase modulation with subsequent pulse compression by a grating pair [8.11]

the red components of the pulse are diffracted into another angle β than the blue ones. From Fig. 8.59 one can infer the path difference S between the plane phase front of the incident wave at point A and the phase plane at point B as

$$S = S_1 + S_2 = \frac{D}{\cos\beta} + \frac{D\sin\gamma}{\cos\beta}\,, \tag{8.55}$$

where D is the distance between the two parallel gratings. From the grating equation

$$d(\sin\alpha - \sin\beta) = \lambda \tag{8.56}$$

for a grating with groove separation α we obtain, after some calculations,

$$\frac{\mathrm{d}S}{\mathrm{d}\lambda} = \frac{\mathrm{d}S}{\mathrm{d}\beta}\cdot\frac{\mathrm{d}\beta}{\mathrm{d}\lambda} = \frac{-D\cdot\lambda}{d^2[1-\lambda/d-\sin^2\alpha]^{3/2}}\,. \tag{8.57}$$

This shows that the optical path length through the grating pair increases with increasing wavelength. Choosing the grating separation D sufficiently large, the broadening of the pulse due to the linear dispersion in the optical fiber can be overcompensated for by the grating pair and leads to a shortening of the duration ΔT of the pulse $I(t)$. The experimental arrangement for the compression of optical pulses after they pass through the fiber is shown in Fig. 8.60.

8.6.4 Measurements of Ultrashort Optical Pulses

Since the time resolution even for fast optical detectors is limited to about 100 ps (except for the streak camera, which reaches 1 ps) the measurement of such short pulses can no longer be performed with conventional devices, but demands new ideas. One method

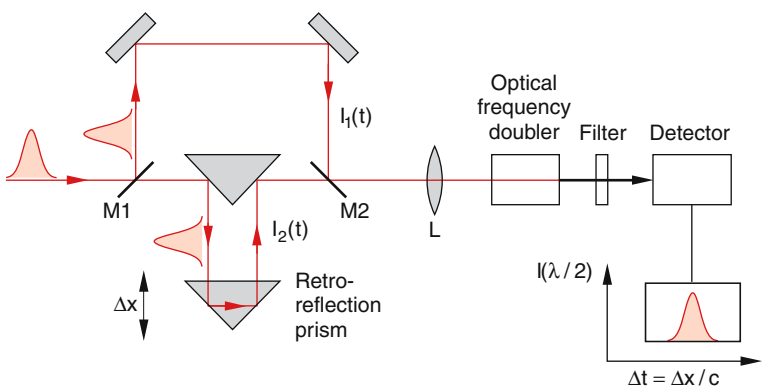

Fig. 8.61. Optical interferometry with translation-retroreflecting prism and second harmonic generation for measuring the width of ultrashort pulses

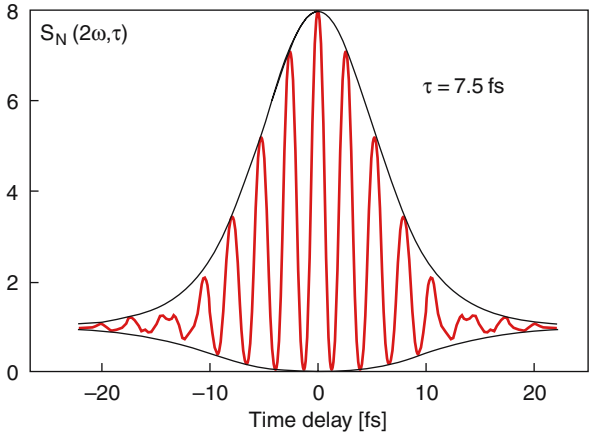

Fig. 8.62. Measured femtosecond pulse with only five optical periods of $T = 2.5$ fs within the full half-width of the envelope

is based on optical interferometry (Fig. 8.61). The laser beam is split into two parts that are recombined after having traveled along two different paths with slightly different path lengths. The superposition of the two parts with variable time delay τ and intensities $I_1(t) = |A_1(t)|^2$ and $I_2(t+\tau) = |A_2(t+\tau)|^2$ gives the total intensity

$$I(\tau) = |A_1(t) + A_2(t+\tau)|^2 \qquad (8.58)$$
$$= I_1(t) + I_2(t) + 2A_1(t) \cdot A_2(t+\tau) ,$$

which depends on the relative phase between the two optical waves, i.e., on the time delay τ. Although the detector cannot follow the fast optical waves, it measures the time dependent interference pattern $I(\tau)$, if the change of the time delay τ is sufficiently slow. If the spectral width of the short pulse is large, it contains a superposition of many monochromatic carrier waves with a nearly continuous frequency spectrum. In this case there will be no clear interference pattern and the detector would measure the sum of the two intensities $I_1 + I_2$, independent on their separation. Here the frequency-doubling of the fundamental wavelength in a nonlinear crystal is a good solution. The intensity

$$\overline{I}(2\omega) \propto |I_1(t) + I_2(t+\tau)|^2$$
$$= \overline{I_1^2} + \overline{I_2^2} + \overline{2I_1(t) \cdot I_2(t+\tau)}$$

of the second harmonics does depend on the time delay τ. Even if the time constant of the detector is long compared to the pulse width and the detector measures the time average of the pulses, it still gives the true pulse profile $I(t)$.

In Fig. 8.62 an actual experimental result is shown for a pulse with 7.5 fs duration (half-width at half-maximum), which shows the optical cycles with 2.5 fs period, monitored with a detector with a time constant of about 1 ns.

Some applications of these ultrashort pulses are discussed in Chap. 12.

SUMMARY

- Laser stands for "**L**ight **A**mplification by **S**timulated **E**mission of **R**adiation".
- A laser consists essentially of three components:
  The *energy pump*, which produces inversion in a medium by selective energy transfer into the medium.
  The *active medium* with a population inversion for selected transitions where an electromagnetic wave passing through the active medium is amplified instead of attenuated.
  The *optical resonator*, which stores the radiation power emitted by the active medium in a few resonator modes. In these modes, the number of photons should be large. This ensures that in these modes the induced emission is much stronger than the spontaneous emission.
- Laser oscillation starts at a threshold power delivered by the pump into the active medium, which depends on the critical inversion and the total losses of the lasing modes. At threshold the losses are just compensated by the gain of the active medium.
- The oscillation frequencies of the laser emission are limited by the spectral range where the active medium has sufficient gain. Within the gain profile of the active medium the lasing frequencies are determined by the eigenresonances of the optical resonator.
- The divergence of the emitted laser beam depends on the number of transverse modes participating in laser oscillation. If only fundamental modes contribute to laser emission, the laser beam profile is Gaussian and its divergence is only limited by diffraction effects.
- Single mode lasers, oscillating on a single fundamental mode, can be realized by additional mode selecting elements inside the laser resonator.
- A synchronous tuning of all frequency-selecting elements allows the realization of a single mode laser with a single wavelength tunable across the spectral gain profile of the active medium.
- The active medium can be a solid, a liquid or a gas. Broad gain profiles are provided by semiconductor materials, by dye solutions, by doped crystals with color centers and by vibronic solid state lasers consisting of an insulator, doped by metal ions.
- For some types of lasers, threshold inversion can only be achieved with pulsed pumps (e. g., pulsed Nd:glass lasers or excimer lasers), while most lasers can be operated in a continuous wave mode (cw lasers) as well as in a pulsed mode.
- The time profile of the laser output is limited by the duration of the pump power above threshold.
- By fast switching of the resonator quality factor, short laser pulses in the nanosecond range can be realized (Q-switched lasers).
- Coupling of many lasing resonator modes (mode locking) results in even shorter pulses down to about 1 picosecond.
- By pulse compression in optical fibers or by nonlinear gain manipulation inside the laser cavity (Kerr lens mode locking) femtosecond laser pulses have been obtained.

PROBLEMS

1. a) What is the population ratio N_i/N_k for atoms in a gas for thermal equilibrium at $T = 300\,\mathrm{K}$, if the wavelength of the transition $E_i \rightarrow E_k$ is $\lambda = 500\,\mathrm{nm}$ and the angular momentum quantum numbers are $J_i = 1$ and $J_k = 0$?
   b) What is relative absorption of a monochromatic light wave per cm path length through a gas, if the transition probability $A_{ik} = 1 \times 10^8\,\mathrm{s}^{-1}$, the gas pressure $p = 1\,\mathrm{mbar}$ and 10^{-6} of all atoms are in the lower state E_k of the transition?
   c) What is the threshold inversion $N_k - N_i$, if the total losses per roundtrip of 10% should be compensated for by the gain over a path length of 20 cm in the active medium?
2. a) Calculate the Doppler-width of the neon line at $\lambda = 633\,\mathrm{nm}$ in a gas discharge with a temperature of $T = 600\,\mathrm{K}$.
   b) How many resonator modes $\mathrm{TEM}_{0,0,q}$ for a resonator length of 1 m can oscillate, if the laser

▶

threshold is at 50% of its maximum value at the line center?

3. An argon laser with a resonator length $d = 1\,\text{m}$, oscillating at a wavelength $\lambda = 488\,\text{nm}$ can be forced to oscillate on a single mode by inserting a Fabry-Perot etalon inside its resonator.
   a) What is the thickness t of the solid fused quartz etalon with a refractive index $n = 1.5$, if only one etalon transmission maximum should lie within the Doppler broadened gain profile of the argon transition at a discharge plasma temperature of $T = 5000\,\text{K}$?
   b) What is the reflectivity R of the two coated planes of the etalon, if the transmission T of the etalon for the neighboring laser resonator modes should decrease to $T = 1/3$ of that for the selected mode with $T = 1$ at the maximum of the etalon transmission?
4. Assume that the two end mirrors of a laser resonator are connected by invar steel rods with a length $d = 1\,\text{m}$ and a thermal expansion coefficient $\alpha = 12 \times 10^{-6}\,\text{K}^{-1}$.
   a) How much does the laser frequency ν shift for a temperature change $\Delta T = 1\,\text{K}$?
   b) If the laser wave inside the resonator passes through 40 cm air at atmospheric pressure, what is the frequency shift for a pressure change of 10 mbar? c) Is the dependence of the cavity's geometric length on the pressure change significant? Give an estimation of this change, using Hooke's law, for the invar rods (the elastic modulus of invar is $E = 10^7\,\text{N/m}^2$, the diameter of the rods is 1 cm).
5. The nearly parallel beam of a laser with wavelength $\lambda = 10\,\mu\text{m}$ and output power of $P = 10\,\text{W}$ has a beam diameter of $d = 3\,\text{cm}$. It is focused by a lens with $f = 20\,\text{cm}$.
   a) How large is the beam waist w_0 in the focal plane?
   b) The intensity distribution in this plane is

$$I(r) = I_0 \times \exp[-(r/w_0)^2]\,.$$

   What is the value of I_0?
   c) Assume that 10% of the laser power can be used for evaporating material from a steel sheet with thickness $t = 1\,\text{mm}$ placed in the focal plane. How long will it take for the laser beam to produce a hole through the steel sheet, if the evaporation heat is $6 \times 10^6\,\text{J/Kg}$?
6. A short Fourier-limited laser pulse ($\Delta t = 10\,\text{fs}$) passes through a medium with refractive index $n = 1.5$ and a dispersion of $\text{d}n/\text{d}\lambda = 4.4 \times 10^4\,\text{m}^{-1}$.
   a) What is the minimum spectral width of the pulse?
   b) After which path length has the width Δt of the pulse doubled due to the linear dispersion of the medium?
   c) How large must the intensity be in order to compensate for the pulse spread caused by the linear dispersion if the nonlinear refractive index is $n_2 = 10^{-10}\,\text{cm}^2/\text{W}$?
7. a) What is the quality factor Q of a laser cavity with mirror separation $d = 1\,\text{m}$, mirror reflectivities $R_1 = R_2 = 0.99$ at a frequency $\nu = 5 \times 10^{14}\,\text{s}^{-1}$, if all other losses (apart from reflection losses) are 2% per roundtrip?
   b) After how much time does the energy stored in the cavity reduce to $1/e$, if at time $t = 0$ the amplification by the active medium suddenly drops to one?
   c) What are the separations $\Delta\nu$ and the half-widths $\delta\nu$ of the longitudinal cavity resonances?
8. Assume the laser oscillation in a cavity mode with $\nu = 4.53 \times 10^{15}\,\text{s}^{-1}$ starts with one photon in this mode. How long does it take until the laser output power in this mode has reached 1 mW, for a net gain g per roundtrip of 5%, a resonator length of $d = 1\,\text{m}$ and mirror transmissions $R_1 = 0$ and $R_2 = 0.02$ if
   a) the net gain $g = -\alpha_0$ is independent of the intensity?
   b) the gain saturation is essential and $\alpha = \alpha_0 + a \times P$ with $a = 0.4\,\text{W}^{-1}\,\text{m}^{-1}$ or $a = 0.55\,\text{W}^{-1}\,\text{m}^{-1}$?